Independence of symmetry breaking on Bem1-mediated autocatalytic activation of Cdc42

Sarah E. Smith,[1,2] Boris Rubinstein,[1] Inês Mendes Pinto,[1] Brian D. Slaughter,[1] Jay R. Unruh,[1] and Rong Li[1,2]

[1]Stowers Institute for Medical Research, Kansas City, MO, 64110
[2]Department of Molecular and Integrative Physiology, University of Kansas Medical Center, Kansas City, KS, 66160

The ability to break symmetry and polarize through self-organization is a fundamental feature of cellular systems. A prevailing theory in yeast posits that symmetry breaking occurs via a positive feedback loop, wherein the adaptor protein Bem1 promotes local activation and accumulation of Cdc42 by directly tethering $Cdc42^{GTP}$ with its guanine nucleotide exchange factor (GEF) Cdc24. In this paper, we find that neither Bem1 nor the ability of Bem1 to bind $Cdc42^{GTP}$ is required for cell polarization. Instead, Bem1 functions primarily by boosting GEF activity, a role critical for polarization without actin filaments. In the absence of actin-based transport, polarization of Cdc42 is accomplished through Rdi1, the Cdc42 guanine nucleotide dissociation inhibitor. A mathematical model is constructed describing cell polarization as a product of distinct pathways controlling Cdc42 activation and protein localization. The model predicts a nonmonotonic dependence of cell polarization on the concentration of Rdi1 relative to that of Cdc42.

Introduction

Actin and microtubule cytoskeletons are key players driving cellular symmetry breaking in diverse morphogenetic systems (Li and Gundersen, 2008). Cytoskeletal polymers, through their inherent structural and biochemical polarity, orchestrate movement and localization of regulatory molecules, which in turn govern cytoskeleton assembly and organization. Such positive feedback loops between structural and regulatory components are features in most models of cell polarization (Wedlich-Soldner et al., 2003; Marco et al., 2007; Seetapun and Odde, 2010; Goehring et al., 2011; Ku et al., 2012; Jose et al., 2013; Slaughter et al., 2013). The budding yeast, however, presents a rather unique case in which cellular symmetry breaking can be accomplished with or without contribution from the cytoskeleton (Ayscough et al., 1997; Irazoqui et al., 2003; Wedlich-Soldner et al., 2004).

Yeast cells naturally bud in a defined pattern, termed bud site selection, guided by sites of previous cell division—bud scars (Casamayor and Snyder, 2002). However, cells are also known to polarize with equal efficiency, albeit in random orientations, when bud scar cues are eliminated or cells lose the ability to recognize them, reflecting a self-organizational mechanism at work. A highly conserved regulator of cellular symmetry breaking and polarized morphogenesis is the small GTPase Cdc42 (Etienne-Manneville, 2004). Localization of Cdc42 from an isotropic distribution around the cortex to a focused cap on one side of the cell is thought to be the key step in symmetry breaking, orchestrating, through Cdc42 effectors, a massive polarized reorganization of cellular components such as the actin cytoskeleton and the secretory machinery, leading to the initiation of polarized growth to generate the bud. The Cdc42 polar cap is dynamically maintained: diffusion of Cdc42 within the membrane and exchange with the fast-diffusing cytosolic pool must be balanced by continuous recycling and retargeting of Cdc42 to the cap region (Wedlich-Soldner et al., 2004; Marco et al., 2007; Slaughter et al., 2009).

Two distinct models have been proposed to explain symmetry breaking in yeast. One model relies on a positive feedback loop between Cdc42-regulated assembly of the actin cytoskeleton and actin cable-mediated transport of exocytic vesicles carrying Cdc42 to the nascent cap (Wedlich-Soldner et al., 2003; Marco et al., 2007). Crucial to this model, recent studies found that membrane microdomains and endocytic corralling serve to maintain Cdc42 concentration in the polar cap (Jose et al., 2013; Slaughter et al., 2013). In normally growing cell populations,

Correspondence to Rong Li: rli@stowers.org

Abbreviations used in this paper: CRIB, Cdc42/Rac-interactive binding; EM-CCD, electron multiplying charge-coupled device; FRET, Förster resonance energy transfer; GEF, guanine nucleotide exchange factor; LatA, Latrunculin A; SC, synthetic complete.

The Rockefeller University Press $30.00
J. Cell Biol.
www.jcb.org/cgi/doi/10.1083/jcb.201304180

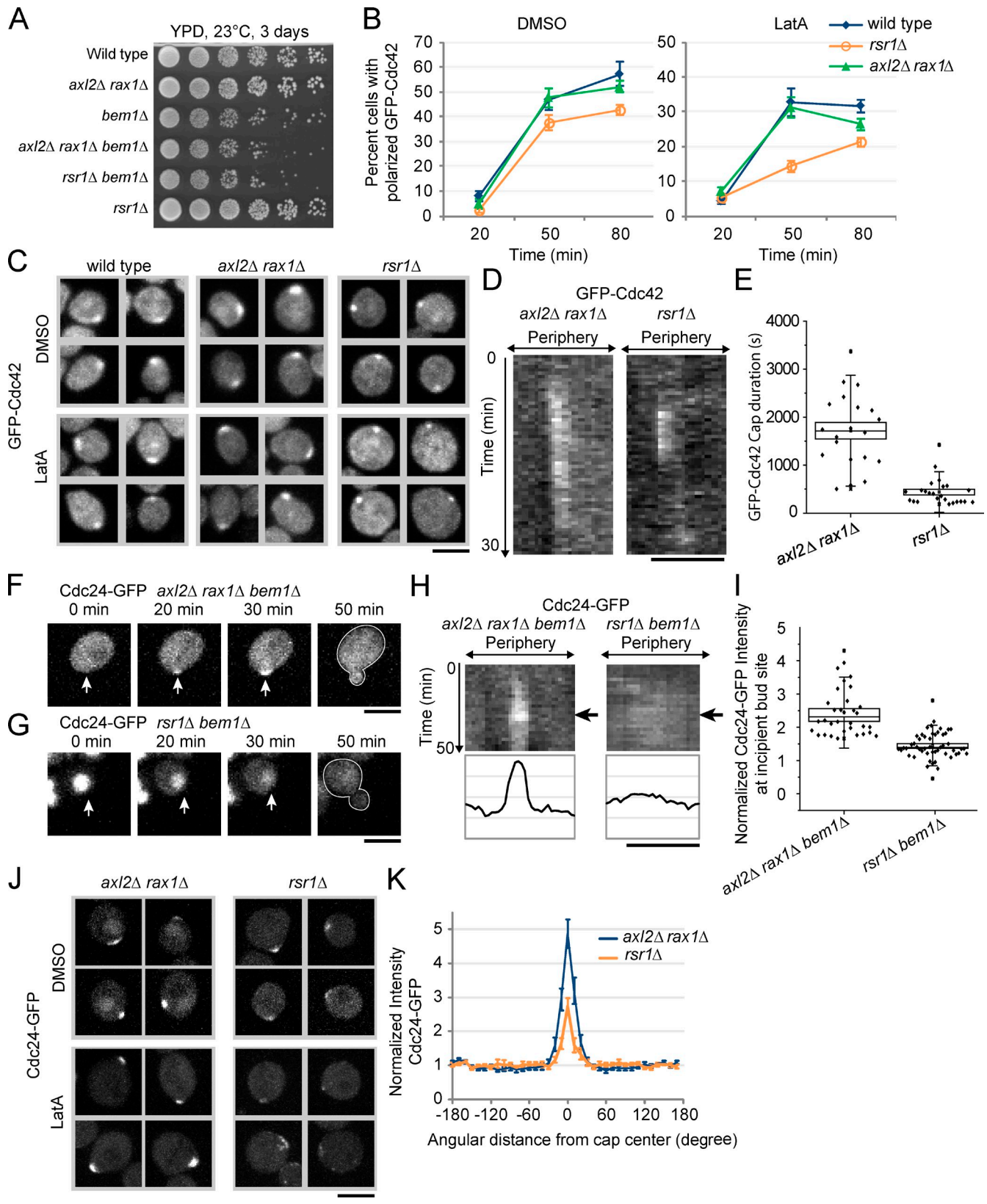

Figure 1. **Bem1 and GEF localization are not required for symmetry breaking.** (A) Cells with indicated genotypes were plated on YPD media and grown at 23°C for 3 d. Cells were grown overnight in liquid culture and then diluted to an OD of 1. This and a series of 10-fold dilution were spotted left to right. (B) Polarization of GFP-Cdc42 wild type, *axl2Δ rax1Δ*, and *rsr1Δ* cells after release from G1 arrest into media containing DMSO or LatA. The percentage of cells with polarized GFP-Cdc42 was determined at different time points (given in minutes) after release. The plots show means from averaging three experiments, and error bars correspond to SEMs. More than 80 cells were counted per time point per experiment. (C) Maximum projections of representative polarized cells from A. (D) Representative kymographs of polarizing GFP-Cdc42 in *axl2Δ rax1Δ* and *rsr1Δ* cells in LatA. Note the unstable polar cap in *axl2Δ rax1Δ* relative to that in *rsr1Δ*. See also Fig. S1 and Videos 1 and 2. (E) Quantification of cap duration in LatA of polarized GFP-Cdc42 in

however, disruption of actin only renders polarization less efficient (Wedlich-Soldner et al., 2004). An actin-independent model for cell polarization is centered on Cdc24, the lone Cdc42 guanine nucleotide exchange factor (GEF) in yeast required for converting Cdc42 into the active, GTP-bound form. Cdc24 has been proposed to form a complex with Bem1 (Peterson et al., 1994; Zheng et al., 1995; Ito et al., 2001), an adaptor-like protein sharing several protein interaction motifs (PB1, SH3, and PX) with animal cell polarity protein PAR6 and the p67Phox adaptor protein in the NADPH oxidase complex. Bem1 also has the ability to bind $Cdc42^{GTP}$ (Bose et al., 2001; Yamaguchi et al., 2007), like PAR6 (McCaffrey and Macara, 2009), as well as effectors of Cdc42 such as the p21-activated kinase Cla4 (Bose et al., 2001). The model posits that positive feedback occurs when the adaptor–GEF complex is recruited to an initial small accumulation of $Cdc42^{GTP}$ through the interaction with Bem1, leading to GEF localization and thus autocatalytic Cdc42 activation at the nascent cap (Butty et al., 2002; Kozubowski et al., 2008). Bem1 was found to be essential for polarization only in the presence of Latrunculin A (LatA), leading to the proposal that Bem1 and actin represent two parallel pathways (Wedlich-Soldner et al., 2004). However, several more recent studies proposed the Bem1-mediated positive feedback loop to be the sole mechanism for symmetry breaking in yeast on the basis of synthetic lethality between *BEM1* and *RSR1*, encoding a Ras-like GTPase required for bud site selection (Kozubowski et al., 2008; Howell et al., 2009). This synthetic lethality was interpreted as to show that Bem1 is required for cell polarization in the absence of bud site selection.

Another unresolved question is how an autocatalytic activation of Cdc42 might lead to polarized localization of Cdc42. Soluble Cdc42 in the cytosol is chaperoned by Rdi1 (Koch et al., 1997; Slaughter et al., 2009; Das et al., 2012). Rdi1, like other Rho GDP dissociation inhibitor proteins, has the ability to extract Cdc42 from the cortex (DerMardirossian and Bokoch, 2005), and this activity is facilitated by modulation of electrostatic interactions of Cdc42 with lipids by the lipid flippase Lem3 (Das et al., 2012). The Rdi1-mediated Cdc42 recycling is required for maintaining the polar cap when actin is inhibited with LatA (Slaughter et al., 2009; Das et al., 2012). Rdi1 may passively facilitate polarization if it is prevented from extracting Cdc42 at the cap through a GEF-dependent mechanism (Kozubowski et al., 2008; Savage et al., 2012), but the rapid, Rdi1-dependent exchange of Cdc42 at the polar cap (Wedlich-Soldner et al., 2004; Slaughter et al., 2009) argues against this idea. In this work, we critically examine the role of Bem1 in symmetry breaking with or without actin and present an alternative model for Cdc42 polarization centered on Rdi1-mediated Cdc42 recycling.

Results

Bem1 is not required for cell polarization in the absence of the bud scar cue

Axial and bipolar budding patterns rely on the trans-membrane markers Axl2 and Rax1–Rax2 complex, respectively (Roemer et al., 1996; Sanders et al., 1999; Kozminski et al., 2003; Fujita et al., 2004; Gao et al., 2007). Transmission of the bud scar signal to Cdc42 requires Rsr1 (Kozminski et al., 2003; Park and Bi, 2007), forming the basis of using *rsr1Δ* as the genetic background for studying spontaneous symmetry breaking. However, Rsr1 may have a more general role in polarization: Rsr1 physically interacts with both Cdc42 (Kozminski et al., 2003) and Cdc24 (Zheng et al., 1995; Park et al., 1997), as well as Bem1 (Park et al., 1997), and deletion of *RSR1* was reported to result in spatially unstable Cdc42 caps (Ozbudak et al., 2005; Howell et al., 2012), particularly in the presence of LatA. Thus, *rsr1Δ* could compromise both bud site selection and the core mechanism of cellular symmetry breaking.

To create a more specific genetic background for studying cellular symmetry breaking, we deleted the bud scar markers Axl2 and Rax1 to remove the structural cues for both axial and bipolar budding, as this leaves the Rsr1 GTPase module intact. We confirmed that *axl2Δ rax1Δ* cells bud in random orientations (Fig. S1 A). Like *rsr1Δ* cells, *axl2Δ rax1Δ* cells grew similarly to the wild type under the standard experimental condition (Fig. 1 A). We next measured the rate of polarization on the population level in the presence or absence of LatA after release from a pheromone-induced G1 arrest. *axl2Δ rax1Δ* cells polarized at rates similar to wild-type cells in both DMSO and LatA. In contrast, *rsr1Δ* cells showed slower polarization in the presence of LatA (Fig. 1, B and C; and Fig. S1 B). Time-lapse imaging was then performed to examine polarization of GFP-Cdc42 in single polarizing *rsr1Δ* or *axl2Δ rax1Δ* cells in LatA. The single-cell analysis revealed a notable difference in polar cap stability between the different mutants: polar caps in *rsr1Δ*

axl2Δ rax1Δ and *rsr1Δ* cells from videos such as the ones shown in D and E. The maximum intensity of the polar caps was measured and plotted over time and was fitted to Gaussian curves. The duration of the cap is reported as the full width half maximum of the Gaussian fit. Boxes, SEM; whiskers, SD; horizontal lines, median values. $P < 10^{-6}$. For each dataset, $n \geq 20$ cells taken from three experiments. (F and G) Time-lapse imaging of Cdc24-GFP in mid–log phase *axl2Δ rax1Δ bem1Δ* (F) and *rsr1Δ bem1Δ* (G) cells. Notice the lack of Cdc24 polarization in G despite successful cell polarization and budding compared with strong Cdc24 polarization in F. Arrows point to incipient bud sites. White outlines indicate the perimeter of the budded cell. See also Videos 3 and 4. (H) Kymographs of polarizing cells from F and G. Shown at the bottom are intensity profiles taken from the time point immediately before bud emergence, indicated in the kymograph by arrows. (I) Quantification of polarization of Cdc24-GFP in *axl2Δ rax1Δ bem1Δ* and *rsr1Δ bem1Δ* cells before bud emergence. Intensity at the emergent bud site is normalized to cortical intensity of the rear half of the cell. Three data points are shown for each cell, corresponding to time points 2, 4, and 6 min before bud emergence. $n = 11$ cells for *axl2Δ rax1Δ bem1Δ* and 17 cells for *rsr1Δ bem1Δ*. Boxes, SEM; whiskers, SD; horizontal lines, median values. $P < 10^{-8}$. (J) Maximum projections of representative cells with polarized Cdc24-GFP in *axl2Δ rax1Δ* and *rsr1Δ* cells in LatA or DMSO. (K) Quantification of polarization of Cdc24-GFP in *axl2Δ rax1Δ* and *rsr1Δ* cells in LatA 50 min after pheromone arrest release from maximum projections of z-stack images. Cells with polarized GFP-Cdc24 were identified, and cortex masks were generated from a separate fluorescent channel (mCherry-Cdc42; see Materials and methods). Mean intensity of the cortex within the mask was determined in 10° increments centered on the polar cap and normalized to the rear half as in I. Normalized profiles were averaged over $n > 18$ cells. Error bars correspond to SEMs. For comparison of values at 0°, $P < 0.001$. Bars, 5 µm.

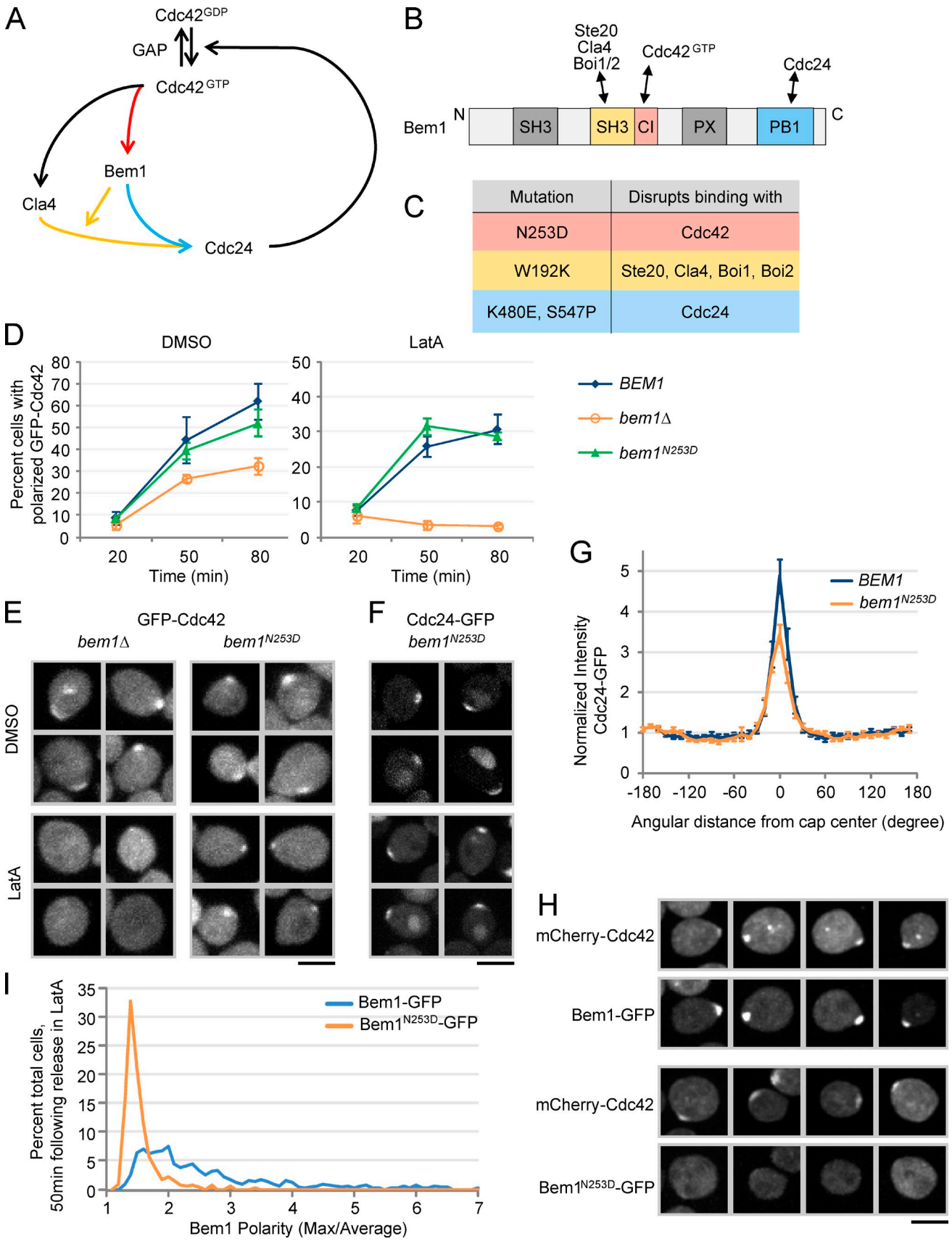

Figure 2. **Bem1–Cdc42^{GTP} binding is not required for GEF localization or cell polarization.** (A) Schematic drawing of the proposed Bem1 feedback loop. (B) Bem1 domains and known interacting partners. (C) Bem1 mutations used in this study and their projected effects on Bem1 interactions. (D) Polarization of GFP-Cdc42 in *axl2Δ rax1Δ BEM1*, *axl2Δ rax1Δ bem1Δ*, and *axl2Δ rax1Δ bem1^{N253D}* cells, as in Fig. 1 B. The plots show means and SEMs from three

lasted for 440 ± 60 s (n = 24) and then sometimes reappeared at a different location (Fig. 1, D and E; Fig. S1 C; and Video 1), whereas *axl2Δ rax1Δ* cells maintained stable polar caps for much longer periods, averaging 1,720 ± 170 s (n = 20; Fig. 1, D and E; Fig. S1 D; and Video 2). This result shows that Rsr1 has a function in symmetry breaking in addition to its role in bud site selection.

Although extensive data were interpreted based on the assumption that Bem1 is required for viability in the *rsr1Δ* background (Kozubowski et al., 2008; Howell et al., 2009, 2012), both *bem1Δ rsr1Δ* double and *bem1Δ axl2Δ rax1Δ* triple mutants are viable and grew similarly to *bem1Δ* alone in the S288c genetic background (Fig. 1 A and Fig. S1 E), suggesting that Bem1 is nonessential for symmetry breaking. Strikingly, time-lapse imaging revealed that *bem1Δ rsr1Δ* cells were able to polarize and bud with severely reduced or unobservable Cdc24 localization to the incipient bud site (Fig. 1, G–I; and Video 3). In contrast, *bem1Δ axl2Δ rax1Δ* cells showed prominent polarization of Cdc24-GFP before bud emergence (Fig. 1, F, H, and I; and Video 4), similar to *bem1Δ* cells as previously reported (Gulli et al., 2000; Butty et al., 2002). Polar localization of Cdc24-GFP in LatA was also significantly reduced in *rsr1Δ* cells compared with *axl2Δ rax1Δ* cells (Fig. 1, J and K). Collectively, these results show that, although Rsr1 and Bem1 together control Cdc24 localization in the polar cap, cells could still polarize and bud without local concentration of the GEF.

Symmetry breaking does not rely on Bem1-mediated Cdc42-to-Cdc24 feedback loop

All existing models assume that Bem1 functions in symmetry breaking by mediating a positive feedback loop connecting Cdc42 and Cdc24 as outlined in Fig. 2 A. Whereas this assumption was supported by gain-of-function experiments in which, for example, Cdc24 covalently linked to Cla4 could bypass the requirement for Bem1 for viability in *rsr1Δ* background (Kozubowski et al., 2008), the assumption has not been rigorously tested using loss-of-function approaches under more physiological settings. To this end, we pursued an unbiased investigation into how Bem1 participates in symmetry breaking by systematically disrupting each of the known physical interactions of Bem1 (Fig. 2 B) using specific point mutations validated in previous studies (Fig. 2 C; Butty et al., 2002; van Drogen-Petit et al., 2004; Yamaguchi et al., 2007). We note that all *bem1* mutants analyzed in the following experiments were in the *axl2Δ rax1Δ* background for observing symmetry breaking in the absence of the bud scar cue.

We began by disrupting the binding of Bem1 to $Cdc42^{GTP}$, a critical step in the proposed Bem1-dependent feedback loop. This was achieved by replacing *BEM1* with a centromeric plasmid expressing *bem1* (under the *BEM1* promoter) bearing the N253D mutation, which lies in the Cdc42 interaction domain and was previously shown to abolish Bem1 binding to active Cdc42 (Yamaguchi et al., 2007). Surprisingly, polarization of GFP-Cdc42 was unaffected in $bem1^{N253D}$ cells in the *axl2Δ rax1Δ bem1Δ* background compared with *BEM1* cells in the same background in the absence or presence of LatA (Fig. 2, D and E). Cdc24-GFP localization was reduced in $bem1^{N253D}$ cells in the *axl2Δ rax1Δ bem1Δ* background in LatA (Fig. 2, F and G) but remained higher than in *rsr1Δ* cells (compare Fig. 2 G with Fig. 1 K). If the N253D mutation indeed disrupted the Bem1–Cdc42 interaction, $Bem1^{N253D}$-GFP should be unable to polarize to the Cdc42 cap. Indeed $Bem1^{N253D}$-GFP polarized poorly (Fig. 2 H), and we quantified the polarization strength of $Bem1^{N253D}$-GFP compared with Bem1-GFP, which indicated a significant ($P < 10^{-64}$) reduction of polarization of $Bem1^{N253D}$-GFP compared with Bem1-GFP (Fig. 2 I). This supports the in vivo disruption of the Cdc42–Bem1 interaction and shows that symmetry breaking does not require localization of Bem1 to the site of Cdc42 accumulation.

Bem1–Cdc24 interaction contributes to polarization by boosting GEF activity

We next disrupted the interaction between Bem1 and Cdc24 mediated through heterodimerization between PB1 domains located at the C termini of these proteins (Ito et al., 2001; Butty et al., 2002). Supporting a crucial role for this interaction in symmetry breaking, mutations in Bem1 abolishing PB1 domain binding ($bem1^{K480E,S547P}$) resulted in failure of cells to polarize in the presence of LatA, whereas polarization in these mutants was only reduced without LatA, similar to that in *bem1Δ* (Fig. 3, A and B).

Because Cdc24 was able to localize even in the absence of Bem1 localization (Fig. 2 F), it was unlikely that the failed polarization of PB1 domain mutant cells was caused by a lack of Cdc24 localization. A previous study hypothesized that Cdc24 exists in an autoinhibited form and that binding by Bem1 might help to relieve this inhibition (Shimada et al., 2004). To investigate this possibility, we developed a Förster resonance energy transfer (FRET)–based biosensor (Itoh et al., 2002; Hodgson et al., 2008) for Cdc42 activation that consists of a linked construct of yeast Cdc42 with the Cdc42/Rac-interactive binding (CRIB) domain from Cla4 (Fig. 4 A), which interacts only with the active, GTP-bound form of Cdc42. These are flanked by GFP and mCherry, such that when the CRIB and $Cdc42^{GTP}$ within the sensor are bound, the GFP and mCherry are brought in close proximity for energy transfer to occur, as illustrated in Fig. 4 A. The polybasic-CAAX box region of Cdc42 was moved

experiments, with n > 80 cells counted per time point per experiment. (E) Maximum projections of representative polarized cells from D. (F) Maximum projections of representative cells with polarized Cdc24-GFP in *axl2Δ rax1Δ* $bem1^{N253D}$ cells after pheromone arrest release in LatA or DMSO. (G) Polarization of Cdc24-GFP in *axl2Δ rax1Δ* cells and in *axl2Δ rax1Δ* $bem1^{N253D}$ cells in LatA, as in Fig. 1 K. For the comparison of peak values at 0°, $P < 0.01$. (H) Localization of Bem1-GFP or $bem1^{N253D}$-GFP in cells with polarized mCherry-Cdc42 after pheromone arrest release in LatA. Z-stack images of representative cells were subjected to a 1 × 1 Gaussian filter before maximum projection. (I) Histogram of Bem1-GFP polarity (maximum pixel intensity/mean pixel intensity per cell) for Bem1-GFP and $bem1^{N253D}$-GFP at 50 min after pheromone arrest release in LatA. n = 520 cells were quantified for each genotype. Bars, 5 µm.

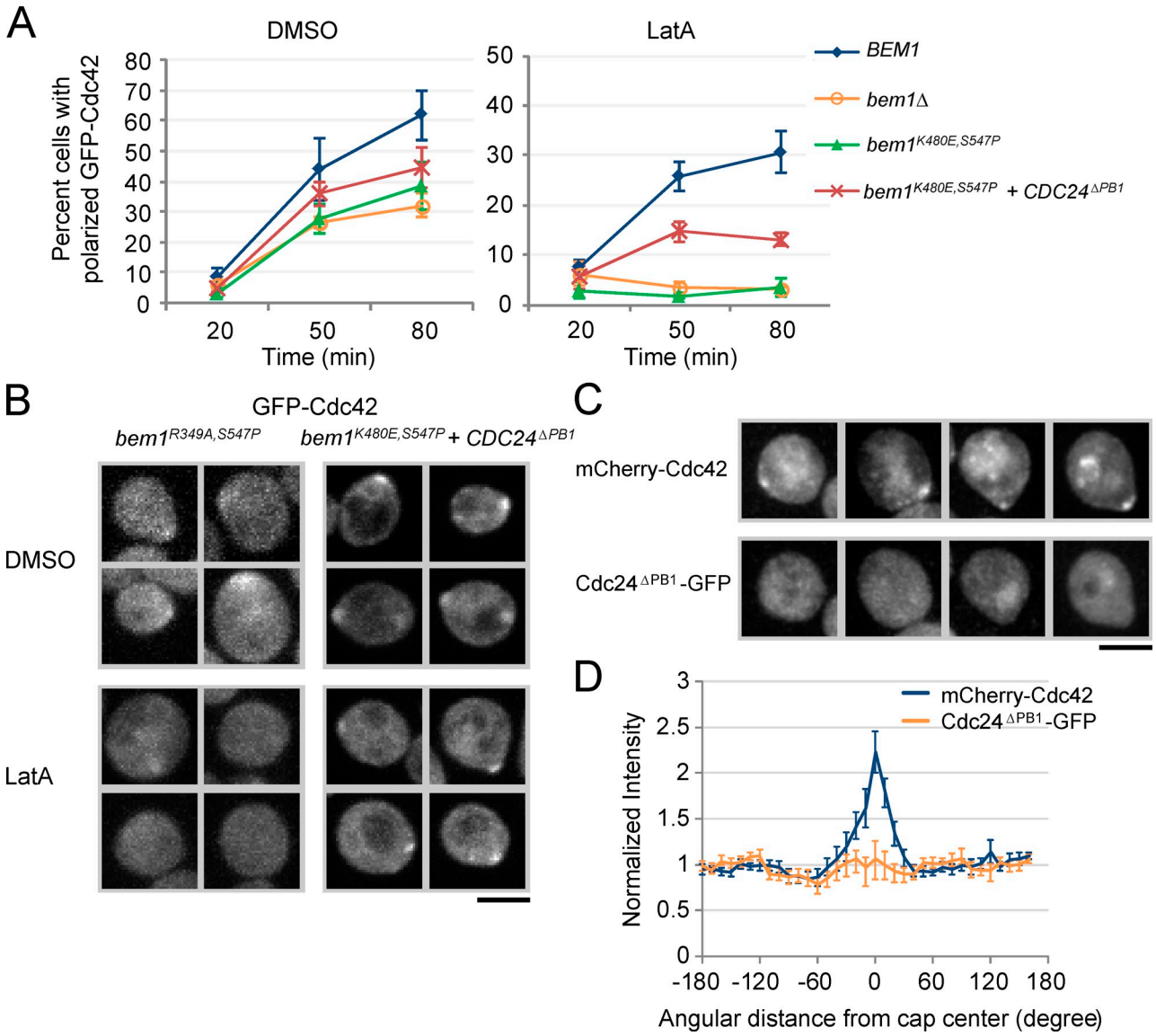

Figure 3. **Bem1 contributes to symmetry breaking by boosting the GEF activity of Cdc24.** (A) Polarization of GFP-Cdc42 in *axl2Δ rax1Δ BEM1* cells, *axl2Δ rax1Δ bem1Δ* cells, *axl2Δ rax1Δ bem1*^{K480E,S547P} cells, and *axl2Δ rax1Δ bem1*^{K480E,S547P} cells expressing *CDC24*$^{\Delta PB1}$ from the *CDC24* promoter. Experimental procedure was as described in Fig. 1 B. The plots show means from averaging three experiments, and error bars correspond to SEMs. More than 80 cells were counted per time point per experiment. (B) Maximum projections of representative cells from A. (C) Localization of Cdc24$^{\Delta PB1}$-GFP in *bem1*^{K480E,S547P} cells with polarized mCherry-Cdc42 after pheromone arrest release in LatA. Z-stack images of representative cells were subjected to a 1 × 1 Gaussian filter before maximum projection. (D) Polarization of Cdc24$^{\Delta PB1}$-GFP and mCherry-Cdc42 in *bem1*^{K480E,S547P} cells in LatA, quantified as in Fig. 1 K for n = 15 cells. Error bars show SEMs. Bars, 5 µm.

C terminally to mCherry to allow proper prenylation and membrane anchorage. Higher FRET efficiency indicates higher net GEF activity toward Cdc42. FRET was measured using the acceptor photobleaching approach as described in the Materials and methods (Fig. 4, A–C; and Fig. S2). Mutations were introduced into the Cdc42 portion of the biosensor, resulting in either a constitutively GTP-bound (Q61L) or GDP-bound (D57Y) state to serve as positive or negative controls, respectively. The positive and the negative controls showed well-separated FRET efficiencies (n > 25 cells for each strain; P < 10^{-8}), whereas the wild-type biosensor showed a FRET level intermediate between the controls as expected (Fig. 4 D).

We introduced the aforementioned Cdc42 activation biosensor into various mutant strains. Deletion of *RSR1* resulted in FRET measurements similar to that in wild-type cells (P = 0.3), whereas deletion of *BEM1* resulted in a significant lower FRET efficiency (P < 10^{-3}; Fig. 4 D). Interestingly, disruption of the Bem1–Cdc24 interaction through the *bem1*^{K480E,S547P} mutation reduced the biosensor FRET by an extent similar to that by *bem1Δ* (P = 0.8 compared with *bem1Δ*, and P < 0.01 compared with *BEM1*; Fig. 4 D). In contrast, GEF activity in *bem1*^{N253D} cells was not significantly different from the wild type (P = 0.4; Fig. 4 D). These results show that the Bem1 interaction with Cdc24 is primarily responsible for enhancement of the latter's GEF activity. Because it was proposed that the PB1 domain of Cdc24 acts as an autoinhibitory domain and that binding by Bem1 may help relieve the autoinhibition (Shimada et al., 2004), deletion of the PB1 domain should result in a constitutively active

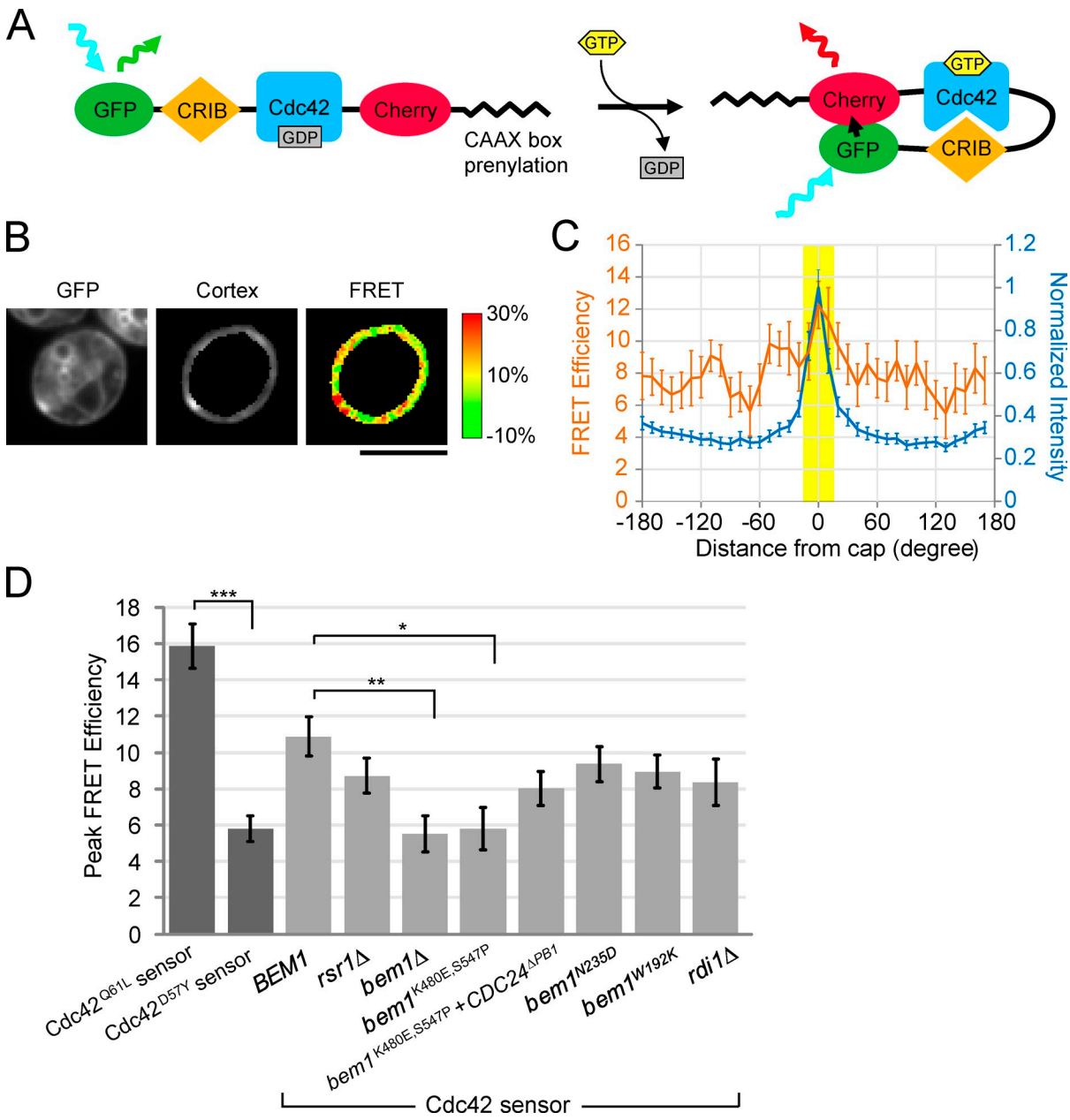

Figure 4. **Biosensor measurements of Cdc24 GEF activity level in various strains.** (A) Schematic representation of the FRET-based biosensor for Cdc42 activation. Active $Cdc42^{GTP}$ binds the CRIB domain, bringing the flanking GFP and mCherry into proximity and allowing FRET. (B) A representative wild-type cell expressing the biosensor containing wild-type Cdc42. Leftmost image shows the sum of the time series for GFP. The center image shows the same image with cortex mask applied (see Materials and methods). The right image shows the FRET efficiency at each pixel within the cell as indicated by the heat bar. Bar, 5 µm. (C) Mean FRET efficiency (orange curve) was measured and plotted in 10° increments along the cortex in the masked image (see B, center image). Mean normalized GFP intensity at the cortex (blue curve) was also measured and plotted. Each plot shows means from >25 cells, and error bars show SEMs. (D) FRET efficiency in the cap region in indicated strains. The left two bars were from wild-type cells expressing positive and negative control sensors. Mean FRET efficiency was measured within the yellow region highlighted in C (see Materials and methods for details). Each histogram shows means from >25 cells, and error bars show SEMs. *, $P < 0.01$; **, $P < 0.001$; ***, $P < 10^{-8}$.

version of Cdc24. Indeed, $Cdc24^{\Delta PB1}$ expressed under the *CDC24* promoter from a centromeric plasmid boosted biosensor FRET in *CDC24* $bem1^{K480E,S547P}$ cells ($P = 0.1$ compared with *BEM1*, and $P < 0.01$ compared with $bem1^{K480E,S547P}$; Fig. 4 D). Importantly, the deregulated GEF ($CDC24^{\Delta PB1}$) partially rescued cell polarization in $bem1^{K480E,S547P}$ cells in the presence of LatA (Fig. 3, A and B), supporting the notion that Bem1's role in cell polarization without actin is mainly mediated through its interaction with Cdc24, which stimulates Cdc24 GEF activity. $Cdc24^{\Delta PB1}$-GFP localized poorly to caps of mCherry-Cdc42 in LatA-treated cells (Fig. 3, C and D), further suggesting that cells can polarize without GEF localization if the overall cortical GEF level is high.

A second mechanism by which Bem1 has been suggested to modulate Cdc24 activity is mediation of complex formation between Cdc24 and the Cdc42 effector Cla4. Cdc24 is hyperphosphorylated by Cla4 in this complex, which requires direct binding of both Cla4 and Cdc24 by Bem1 (Gulli et al., 2000;

Bose et al., 2001; Wai et al., 2009). Expression of a fusion construct of $Cdc24^{\Delta PB1}$ linked with Cla4 was shown to rescue the synthetic lethality of *Δrsr1 Δbem1* in the yeast strain background used in a previous study (Kozubowski et al., 2008), which was interpreted as supporting a sufficiency of complex formation between Cdc24 and Cla4 for symmetry breaking. However, we found that the rescued cells failed to polarize in the presence of LatA (Fig. 5, A and B), suggesting that the fusion construct relies on an actin-dependent mechanism to accomplish the rescue. Because Bem1 and Cla4 interact through the Bem1 SH3 domain and a proline-rich motif in Cla4 (Bender et al., 1996), we tested the disruption of the projected Bem1–Cla4–Cdc24 complex by mutating the invariant tryptophan ($bem1^{W192K}$) in the SH3 domain required for binding to proline-rich motifs (Larson and Davidson, 2000). $bem1^{W192K}$ resulted in a slight but significant (P = 0.05 at 50 min) reduction in the percentage of polarized cells in the presence of LatA compared with the control (Fig. 5, C and D), but biosensor measurements showed GEF activity similar to that in the wild-type polar cap (P = 0.3; Fig. 4 D). Importantly, the localization of Cdc24 was also normal in the $bem1^{W192K}$ background (Fig. 5, E and F). These results suggest that GEF localization and activity at the polar cap is largely independent of the interaction of Bem1 with its SH3 domain ligands. It is interesting to note that $bem1^{W192K}$ mutant cells frequently displayed two polar caps in LatA, suggesting that the affected interaction is important for the singularity of the polar axis in the absence of actin, but further investigation of this phenomenon is beyond the scope of this work.

Symmetry breaking without actin requires Rdi1-mediated cytosolic targeting of Cdc42

If not through the Bem1 feedback loop, how then does Cdc42 polarize without actin? In addition to the membrane-bound pool, which is targeted by actin, Cdc42 exists in the cytosol in a soluble pool as the Rdi1-bound complex (Koch et al., 1997; Tiedje et al., 2008; Slaughter et al., 2009). Consistent with a new study published recently (Freisinger et al., 2013), *rdi1Δ* cells fail to polarize Cdc42 in the presence of LatA after release from pheromone G1 arrest (Fig. 6, A and B), suggesting that targeting from the Rdi1-bound cytosolic pool is not only required for maintaining but also for establishing Cdc42 protein polarization when actin is disrupted. The polarization defect in *rdi1Δ* cells in the presence of LatA was not caused by insufficient GEF activity: biosensor measurements indicated the GEF activity in *rdi1Δ* cells to be similar to that in the wild type (P = 0.89; Fig. 4 D), and expression of $Cdc24^{\Delta PB1}$ did not rescue the polarization defect of *rdi1Δ* cells (Fig. 6, A and B). Furthermore, deletion of *RDI1* did not affect growth of *rsr1Δ* or *axl2Δ rax1Δ* cells, suggesting that Rdi1 is not required for cellular symmetry breaking when actin is intact. However, deletion of *RDI1* exacerbated the slow growth and polarization phenotypes in *bem1Δ* cells (Fig. 6, A and C). Collectively, the aforementioned results show that targeting of Cdc42 from the cytosolic Rdi1-bound pool is central to Cdc42 polarization in the absence of actin-based vesicular trafficking and that this process is distinct from GEF activation, which does not have to be spatially confined.

Analytical model of actin-independent asymmetry breaking without localized GEF activation

As a theoretical exploration of the polarization mechanism based on findings of this study, we used a minimalistic approach (Goryachev and Pokhilko, 2006; Otsuji et al., 2007; Altschuler et al., 2008; Mori et al., 2011) to discover the conditions that could allow symmetry breaking through Rdi1-mediated Cdc42 targeting from the cytosol but not local activation of the GEF. Main components of the 1D model include Cdc42 on the membrane (local concentration $u(x,t)$), a fraction ($a_1 < 1$) of which is in the active GTP-bound form, Cdc42 in cytosol $v(x,t)$, free (cytosolic) Rdi1 $R_f(x,t)$, and the cytosolic Rdi1–Cdc42 complex $R_c(x,t)$. Considering the simplest case in which the activity G that dissociates the Rdi1–Cdc42 complex is proportional to squared density of active Cdc42, $G(u) = a_2(a_1u)^2$, i.e., $G(u) = Au^2$, in which $A = a_2a_1^2$; the membrane targeting term for Cdc42 then reads Au^2R_c (Fig. 7 A). Cdc42 internalization is given by the term βuR_f, in which β is the extraction rate of membrane-bound Cdc42 by free Rdi1. Because cytosolic Cdc42 exists in Rdi1- and vesicle-bound states (Das et al., 2012; Slaughter et al., 2013), we assume $R_c = \gamma v$, in which $0 < \gamma < 1$. Based on recently published data on the mobile pools of Cdc42 by using fluorescence correlation spectroscopy (Das et al., 2012), γ was estimated to be 0.4. Using the conservation condition for mean concentration of Rdi1 (R) in the cell, we have $R_f = R - R_c = R - \gamma v$.

The cell is represented as a line segment with a size L. Dynamics of the Cdc42 concentrations are described in the region $0 \le x \le L$: $\partial u/\partial t = \gamma A(u - u_b)^2v - \beta(u - u_b)(R - \gamma v) + D_u(\partial^2u/\partial x^2)$, and $\partial v/\partial t = -\gamma A(u - u_b)^2v + \beta(u - u_b)(R - \gamma v) + D_v(\partial^2v/\partial x^2)$, in which u_b denotes a nonzero but small basal uniform concentration of Cdc42 in the membrane (see Supplemental material). The diffusion of Cdc42 in the cytosol is much faster than that in the membrane: $D_v >> D_u$. The equations are subject to no-flux boundary conditions, and the total amount CL of Cdc42 in the cell is conserved. A linear stability analysis showed that the growth rate of small perturbations to an initial uniform distribution is proportional to the activation level of Cdc42 (see Supplemental material). Simulations of the model showed the perturbations lead to growth of a single peak of Cdc42 to a steady level (Fig. 7 B).

We explored the parameter space for R (cellular Rdi1 level) and A (essentially a parameter describing the activation level of Cdc42 that also impacts Cdc42 targeting) required for symmetry breaking. For a fixed value of A, simulations showed that formation of stable polarity responds nonmonotonically to R, such that polarization occurs when R is in the range of 0.5–0.8 (note R values are normalized to the global concentration of Cdc42, $C = 1$, and the upper but not lower boundary depends on the value of A; see Discussion). When R is above this range, no polarization occurs as a result of a lack of Cdc42 targeting to membrane, whereas when R is below the range, a high level of Cdc42 uniformly distributes on the membrane (Fig. 7 C). To perform a qualitative experimental test of this prediction, we induced expression of Rdi1 under the *GAL1* promoter for varying time periods before release from pheromone arrest into LatA-containing media (Fig. S3 A).

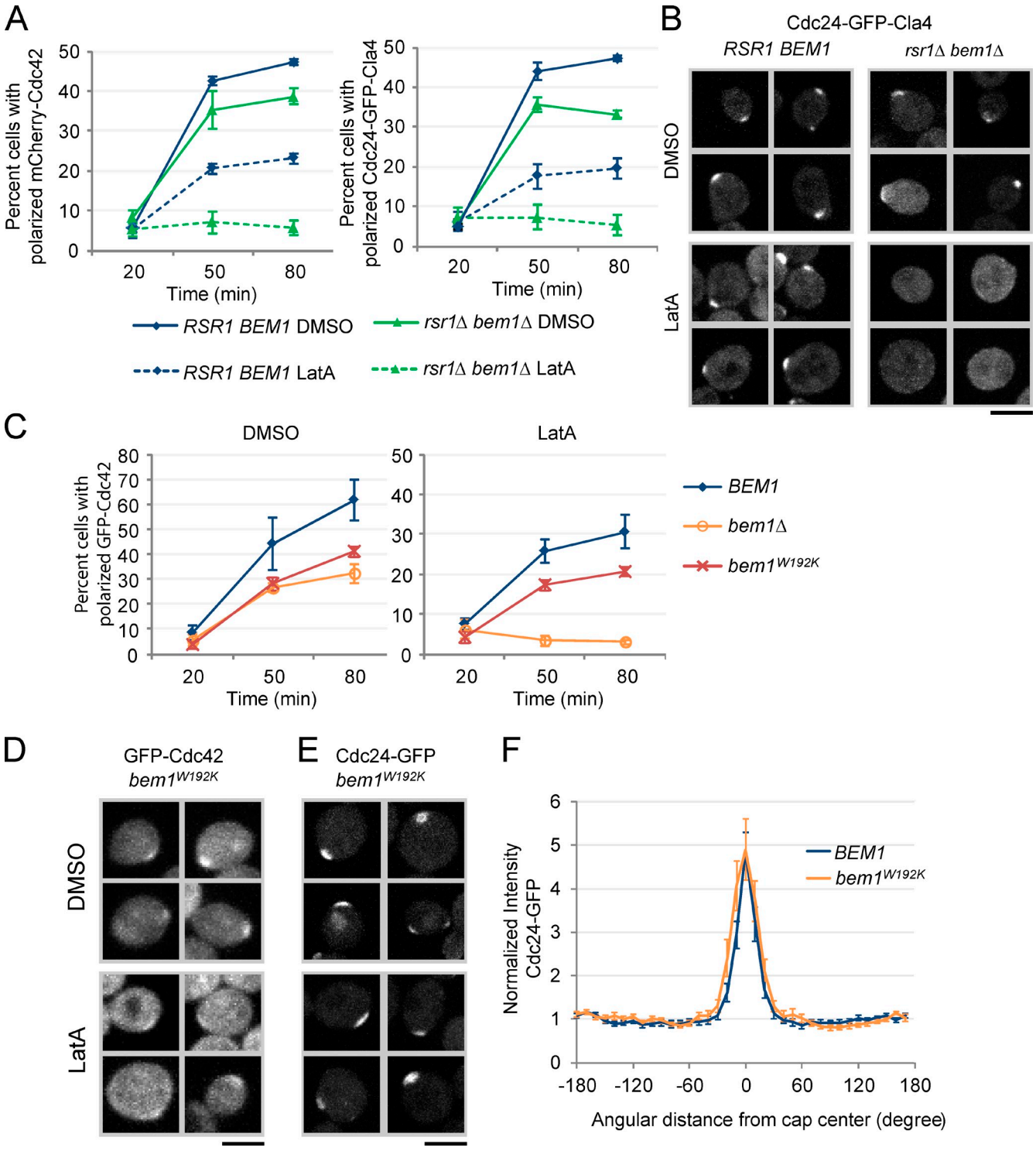

Figure 5. **The Bem1–Cla4 interaction is not required for Cdc24 localization or symmetry breaking.** (A) Polarization of mCherry-Cdc42 (left) and Cdc24$^{\Delta PB1}$-GFP-Cla4 (right) in *RSR1 BEM1* cells and in *rsr1Δ bem1Δ* cells in DMSO or LatA upon release from G1 pheromone arrest. Experimental procedure was as described in Fig. 1 B. The plots show means from averaging three experiments, and error bars correspond to SEMs. More than 80 cells were counted per time point per experiment. (B) Maximum projections of representative cells from A. (C) Polarization of GFP-Cdc42 in *axl2Δ rax1Δ BEM1* cells, *axl2Δ rax1Δ bem1Δ*, and *axl2Δ rax1Δ bem1*^{W192K} cells, as in Fig. 1 B. (D) Maximum projections of representative polarized cells from C. (E) Maximum projections of representative cells with polarized Cdc24-GFP in *axl2Δ rax1Δ bem1*^{W192K} cells after pheromone arrest release in LatA or DMSO. (F) Quantification of Cdc24-GFP polarization in *axl2Δ rax1Δ* cells and in *axl2Δ rax1Δ bem1*^{W192K} cells, as in Fig. 1 K. For the comparison of peak values at 0°, P = 0.5. Plots show normalized profiles averaged over $n > 17$ cells. Error bars correspond to SEMs. Bars, 5 µm.

Quantifying the percentage of polarized cells at 50 min after the release, it was apparent that cell polarization occurs optimally at the concentration of Rdi1 induced for 60 min with galactose and declines sharply above and more gradually below this expression level (Fig.7 D). Measurement of mean fluorescence intensities of Rdi1-GFP and GFP-Cdc42, each expressed

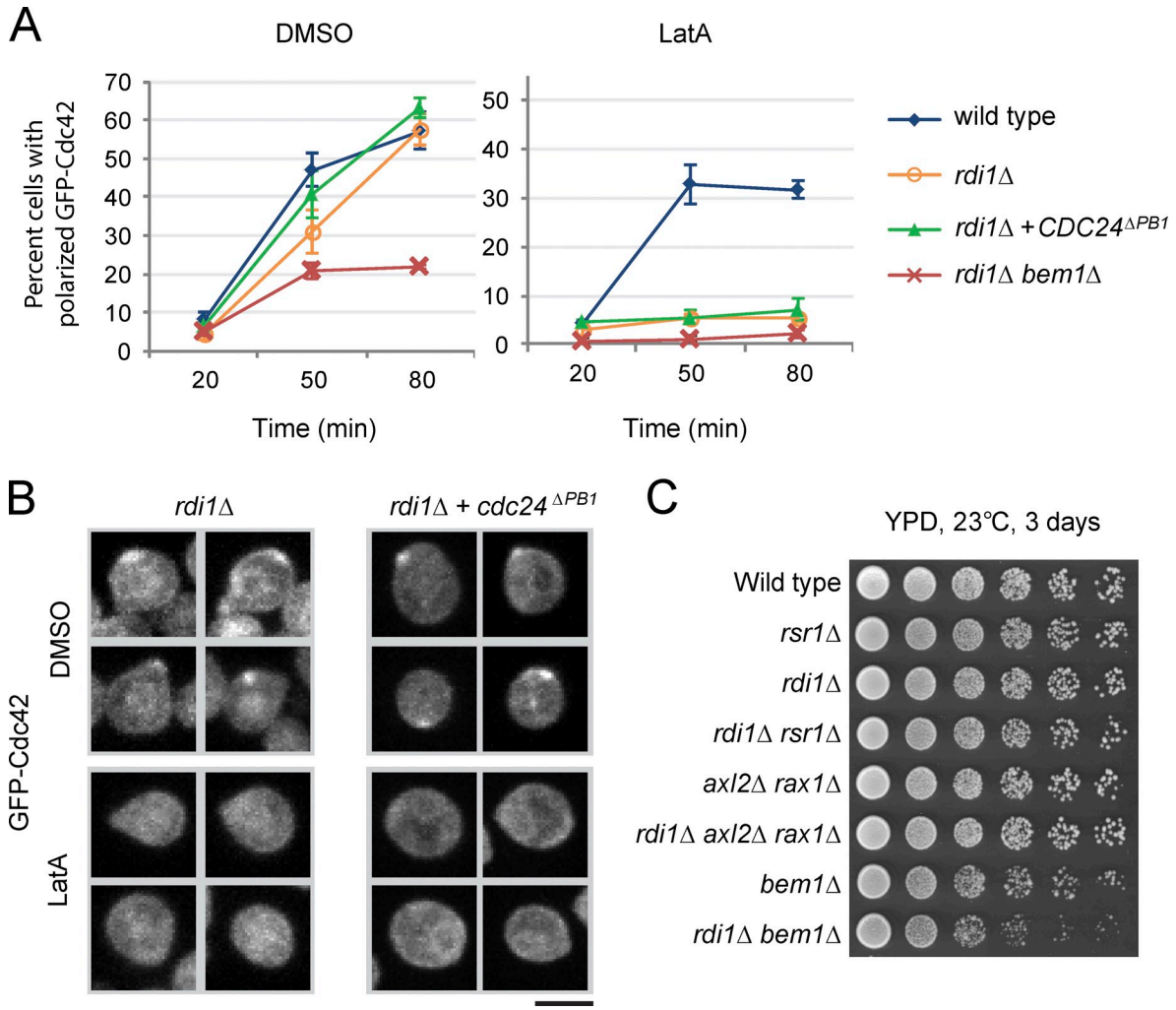

Figure 6. **Rdi1-mediated cytosolic targeting of Cdc42 is essential for symmetry breaking without actin.** (A) Polarization of GFP-Cdc42 in wild-type cells, *rdi1Δ* cells, *rdi1Δ* cells expressing *CDC24*$^{\Delta PB1}$ from the *CDC24* promoter, and *rdi1Δ bem1Δ* cells in DMSO or LatA after release from G1 pheromone arrest. Experimental procedure was as described in Fig. 1 B. The plots show means from averaging three experiments, and error bars correspond to SEMs. More than 80 cells were counted per time point per experiment. (B) Maximum projections of representative cells from A. Bar, 5 µm. (C) Serial dilution of cells with the indicated genotypes from an overnight culture with an OD of 1 were plated on YPD media and grown at 23°C for 3 d.

under its endogenous promoter, confirmed that Rdi1 concentration is ∼0.6-fold of that of Cdc42, within the allowable range for symmetry breaking (Fig. S3 B). We also fixed the value of *R* and varied *A* and found that symmetry breaking requires a threshold level of Cdc42 activation (Fig. 7 E), which is qualitatively consistent with the experimental findings in Fig. 3 (see Discussion).

Discussion

Distinct pathways of Cdc42 activation and localization contribute to symmetry breaking

The aforementioned results indicate that mechanisms of Cdc42 localization and activation are not obligatorily coupled. In any single location on the cortex, induction of downstream events or feedback circuits that rely on Cdc42 effectors depends on the concentration of Cdc42^{GTP}, a product of two factors: (1) total Cdc42 protein concentration (controlled by localization on the cortex) and (2) relative abundance of the GTP-bound state of Cdc42 (controlled by GEF/GAP balance) in that location. Modulation of either factor can be envisioned to affect the local Cdc42^{GTP} level and therefore the capacity for initiating the downstream reactions required for symmetry breaking (Fig. 8). This concept is sufficient to interpret all the experimental observations made in this study. Specifically, our results show that when both the actin-based vesicular trafficking and Rdi1-dependent cytosolic targeting mechanisms are intact, symmetry breaking, although less efficient, occurs even without strong GEF localization or the benefit of Bem1's GEF boosting ability (Fig. 8 B). Alternatively, optimal GEF activation may compensate for suboptimal protein localization such as in the case of actin disruption with LatA (Fig. 8 C). However, when both activation and protein targeting are inhibited to a certain degree, such as the combination of *bem1Δ* and actin inhibition, the threshold of Cdc42^{GTP} concentration could not be achieved to enact the downstream reactions and positive feedback loops for symmetry breaking (Fig. 8 D).

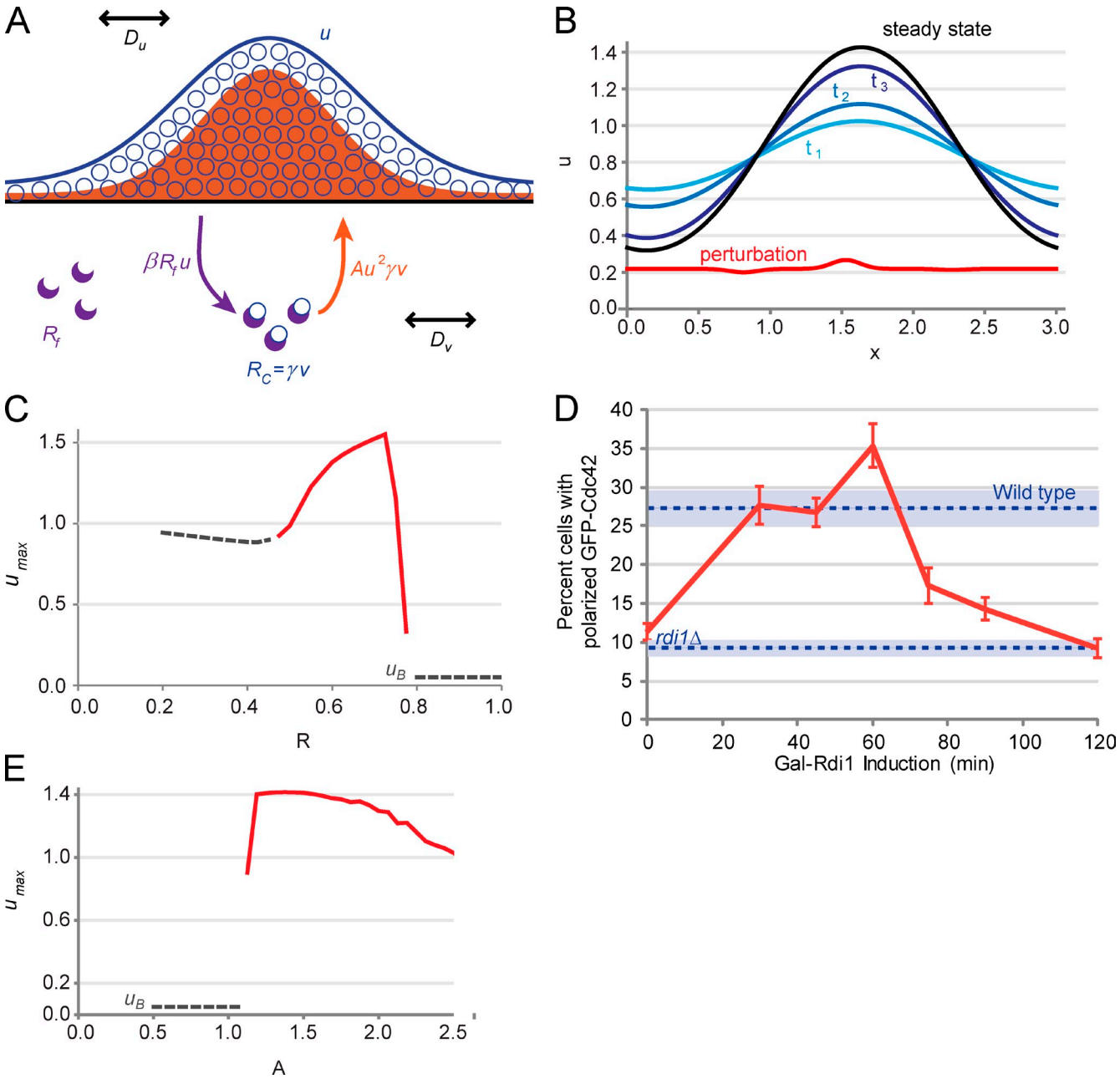

Figure 7. **Mathematical model of Rdi1-dependent symmetry breaking and parameter validation.** (A) Schematic of analytical model for Rdi1-dependent polarization. Distribution of Cdc42 across the cortex is given by $u(x,t)$ (blue curve), of which a constant fraction a_1 is activated. Cdc42 extraction is proportional to free Rdi1, R_f (purple crescents), and $u(x,t)$ by a constant β. Targeting of Cdc42 to the cortex is assumed to be proportional to the squared distribution of active $Cdc42^{GTP}$, $(a_1u)^2$, the profile of which is represented by the filled orange curve. Cytosolic diffusion D_v and cortical diffusion D_u are shown in black. (B) Simulation of cell polarization via the Rdi1-dependent mechanism. Initial distribution of cortical Cdc42 at the time of perturbation is shown in red, with steady-state shown in black and intermediate time points given in blue. The parameter values used in the simulation shown are $C = 1$, $\gamma = 0.4$, $\beta = 0.2$, $D_v = 0.1$, $D_u = 0.01$, $u_b = 0.05$, $L = 3$, $A = 1.75$, and $R = 0.6$. (C) Simulated data for Rdi1-dependent polarization, showing dependence of polarization strength u_{max} on R, and Rdi1 concentration relative to Cdc42. Gray dashed lines indicate cortical Cdc42 concentration in unpolarized states, whereas the red curve indicates mean u_{max} over 25 simulations for parameter values in which polarization is allowed. The parameter values are as in B, with changing value of R. (D) Experimental assessment of the impact of Rdi1 expression level on polarization without actin. Expression of Rdi1 was induced under the *GAL1* promoter for the indicated amounts of time (x axis) concurrent with a 1-h G1 pheromone arrest followed by a 0.5-h pheromone arrest in glucose media before release into LatA-containing media (see diagram in Fig. S3). The percentages of polarized cells were counted at 50 min after release. P = 0.06, comparing polarization in wild type with that of 60-min galactose (Gal) induction. The plots show means from three experiments, and error bars correspond to SEMs (blue shading indicates error bars for controls). More than 80 cells were counted per time point per experiment. (E) Simulated data for Rdi1-dependent polarization, showing dependence of polarization strength u_{max} on A. Gray dashed lines indicate cortical Cdc42 concentration in unpolarized states, whereas the red curve indicates mean u_{max} over 25 simulations for parameter values in which polarization is allowed. The parameter values are as in B, with $R = 0.6$ and changing value of A.

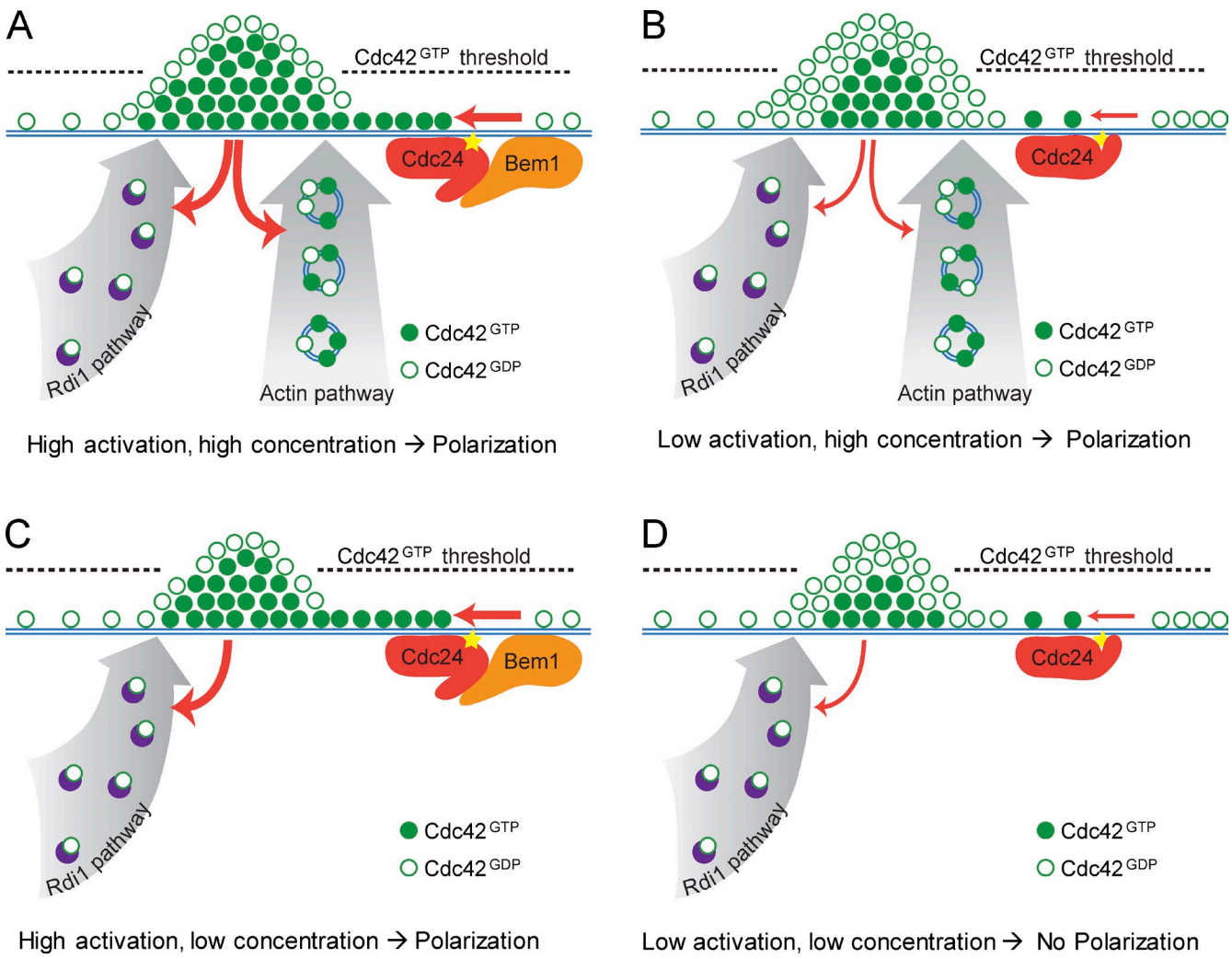

Figure 8. **A schematic explanation of the phenotypic observations based on the cooperation between Cdc42 targeting and activation.** The concentration of active $Cdc42^{GTP}$ (filled green circles) on the cortex is a fraction of total Cdc42 (filled and open green circles) determined by the GEF activity of Cdc24 boosted by Bem1. Cdc42 localization is controlled by both actin-dependent vesicle (blue circles) trafficking and Rdi1-dependent (purple crescents) pathways. Local concentration of active $Cdc42^{GTP}$ must reach a threshold level (dotted lines) before imposing sufficient feedback for symmetry breaking. (A) Wild-type cells—both Cdc42 activity and localization are maximized. The level of $Cdc42^{GTP}$ is well above the threshold. (B) *bem1Δ* cells—GEF activity is reduced but with the localization of total Cdc42 remaining high, the threshold level of $Cdc42^{GTP}$ is still attained. (C) LatA-treated wild-type cells–elimination of the actin-based target pathway reduces localization of Cdc42, but with high activation, the $Cdc42^{GTP}$ threshold can still be reached. (D) LatA-treated *bem1Δ* cells—decreasing both the activation level and the localization of total Cdc42 prevents attainment of the threshold level of $Cdc42^{GTP}$ for symmetry breaking.

The function of Bem1 in cellular symmetry breaking

The previous conclusion that Bem1 is essential for symmetry breaking was built on the synthetic lethal interaction between *bem1Δ* and *rsr1Δ* and the implicit assumption that *rsr1Δ* affects only bud site selection but not the core symmetry-breaking mechanism. The results presented here and in previous studies (Ozbudak et al., 2005; Howell et al., 2012) have shown that Rsr1's function is beyond bud site selection but that *bem1Δ* or *bem1Δ rsr1Δ* double mutant cells are capable of polarization as long as actin is intact. Our approach of interaction-specific perturbation by using point mutations has revealed different, as opposed to concerted, functions for the various Bem1-mediated interactions in cell polarization. The mutant analysis shows that the Bem1–Cdc42 interaction is important for localization of Bem1 to the polar cap, but this is neither crucial for Cdc24 localization nor required for symmetry breaking with or without actin. This result also implies that Bem1 can fulfill its main function in symmetry breaking without itself being localized. In contrast, disruption of the Bem1–Cdc24 interaction prevented symmetry breaking only when actin was inhibited. This defect correlates with significantly reduced GEF activity and can be rescued by a Cdc24 construct that enhanced GEF activity but was unable to localize. These results strongly suggest that a key function of Bem1 is to boost the GEF activity of Cdc24 globally or locally.

Bem1 binding was also thought to enhance GEF activity by bridging a complex between Cdc24 with the p21-activated kinase Cla4, thus facilitating Cdc24 hyperphosphorylation. Although mutagenesis of as many as 38 phosphorylated sites on Cdc24 did not result in any observable phenotype (Wai et al.,

2009), disruption of Bem1 SH3 domain binding to polyproline motifs via the *bem1*^{W192K} mutation resulted in a partial decrease in polarization efficiency in the presence of LatA (Fig. 5 C). However, as the *bem1*^{W192K} mutation would also disrupt the interaction with Boi1 and Boi2, which are together required for viability (Bender et al., 1996), the effect of this mutation does not permit simple interpretation. Nevertheless, we speculate that, in addition to GEF activation, Bem1 functions as a bona fide adaptor with multiple weak ligand interactions to enhance the affinity of protein complexes required for robust cell polarization.

The emerging role of Rdi1 and Rsr1 in cellular symmetry breaking

Our results show that Rdi1 plays a critical role in actin-independent polarization of Cdc42, consistent with a recent study (Freisinger et al., 2013). As a Rho GDP dissociation inhibitor, Rdi1 is the cytosolic chaperone of prenylated Cdc42 and thus governs the targeting of this pool of Cdc42 to the site of polarization. Our previous work showed that Rdi1 is required for rapid recycling of Cdc42 that helps maintain a dynamic polarized Cdc42 concentration in the presence of significant membrane diffusion (Slaughter et al., 2009; Das et al., 2012). To recycle Cdc42 back to the polar cap, however, the Rdi1–Cdc42 complex must be broken apart, and what catalyzes this reaction remains a key missing link in the cytosolic Cdc42-targeting pathway. We envision that to enable symmetry breaking via this cytosolic targeting pathway, active Cdc42 on the plasma membrane controls the dissociation of the Rdi1–Cdc42 complex in some manner, restricting Cdc42 anchoring to sites of prior Cdc42 accumulation. Modeling of experimentally observed Cdc42 dynamics during steady-state polarity predicted that the window of targeting Cdc42 from the cytosolic complex must overlap with that of actin-based delivery (Slaughter et al., 2009), but the biochemical mechanism underlying this spatial restriction remains unknown.

The Ras-like GTPase Rsr1 has long been known to be essential for bud site selection, but our results, as well as the finding presented in several previous studies (Park et al., 2002; Kozminski et al., 2003; Kang et al., 2010), indicate that its role in polarization is more extensive and central to symmetry breaking than previously thought. Although Rsr1 is not strictly required for polarization, especially when actin is intact, in its absence, the established polar cap exhibits drastically reduced spatial and temporal stability, as shown in this and previous studies (Ozbudak et al., 2005; Howell et al., 2012). Previous studies attributed this instability to GAP-mediated negative feedback, and if so, Rsr1 may locally regulate this negative feedback to enhance the stability of the polar cap. The finding that Bem1 and Rsr1 share a role in Cdc24 localization provides an alternative explanation for the previously reported synthetic lethality of *bem1Δ* and *rsr1Δ*: perhaps in some yeast strain background, without GEF localization, *bem1Δ rsr1Δ* cells are unable to achieve a sufficient level of cortical Cdc42^{GTP} to initiate the feedback that brings about symmetry breaking.

A new model of cytoskeleton-independent symmetry breaking

Models of yeast cell polarity have focused on achieving a stable, nonuniform distribution of Cdc42 on the membrane (Onsum and Rao, 2009). Existing models are mass-conserved reaction-diffusion models (Goryachev and Pokhilko, 2006; Otsuji et al., 2007; Altschuler et al., 2008; Mori et al., 2011). Analysis of these models showed that the polarization is caused by Turing-type instability (Rubinstein et al., 2012), the physical reason for which lies in the significant difference in the Cdc42 diffusion constants in the cytosol and in the membrane, in addition to specific nonlinear dependence of protein recruitment on the local concentration of Cdc42 in the membrane. A major feature of the Turing instability is that a stable state of the two-component system may become unstable in the presence of diffusion. Cdc42 concentrations in the cytosol and on the membrane are considered as "master" variables, whereas concentrations of other proteins are consequences of the master variable dynamics.

One model introduced by Goryachev and Pokhilko (2008), which formed the basis for subsequent studies (Howell et al., 2012; Savage et al., 2012), assumes that polarization occurs via a mechanism of autocatalytic activation of Cdc42 through recruitment of the Bem1–Cdc24 complex. Rdi1 was incorporated into the model as a passive aide in Cdc42 recycling, prevented through a GEF-dependent mechanism from extracting Cdc42 at the cap. The authors considered a complex model consisting of eight reaction-diffusion equations for dynamics of membrane bound and cytoplasmic proteins diffusing in 2D and 3D, respectively (Goryachev and Pokhilko, 2008). Using several simplifying assumptions, they reduced the original model to a 1D version for the master variables only. Both the full and the reduced models produced qualitatively the same results showing the existence of robust clustering of Cdc42 on the membrane. In our approach, we focused on the development of the minimalistic 1D model designed to grasp major features of the actin-independent polarization process.

Our model differs mechanistically from that of Goryachev and Pokhilko (2008) in the lack of reliance on autocatalytic activation of Cdc42 via a proposed Bem1–Cdc42–Cdc24 complex. Rather, symmetry breaking is achieved through autocatalytic Cdc42 protein recruitment from the cytosolic Rdi1–Cdc42 complex. We demonstrate through both model simulation and experimental measurements that symmetry breaking depends on a window of Rdi1 concentration relative to that of Cdc42. In contrast, cells have more permissive requirements on the level of GEF activity, such that although a threshold level is required, higher levels are well tolerated. This explains the main experimental findings that cell polarization can occur with varying degrees of GEF concentration in the polar cap and that *bem1* mutations that impair GEF activation are more detrimental to polarization when cells are reliant on the Rdi1-based targeting pathway (i.e., when the actin-based transport pathway is disabled).

In summary, a key insight resulting from the analyses performed in this work is that activation and localization of Cdc42 are achieved via distinct mechanisms that contribute quantitatively and productively to symmetry breaking. Although both aspects of Cdc42 regulation are required, partial deficiency in either may be compensated as a result of the presence of multiple mechanisms achieving the other. This cooperation underscores both the complexity and robustness of the yeast cell polarity system.

Materials and methods

Detailed model description

We considered a 1D model describing Cdc42 protein dynamics in a yeast cell undergoing symmetry breaking transition from a uniform state to a polarized state. For the actin-independent pathway, we introduce the following components of the model: Cdc42 on the membrane (local concentration $u(x,t)$) with active fraction $a_1 < 1$, Cdc42 in cytosol $v(x,t)$, free (cytosolic) Rdi1 $R_f(x,t)$, protein complex Rdi1–Cdc42 $R_c(x,t)$, and a certain activity $G(u)$ leading to breaking up of the complex into free Rdi1 and membrane-anchored Cdc42. We considered the simplest case when this activity is proportional to squared density of active membrane Cdc42, i.e., $G(u) = a_2a_1^2u^2 = Au^2$, in which $A = a_2a_1^2$.

The membrane targeting term reads $G(u)R_c$, and the internalization term is βuR_f, in which β is the extraction rate. Assuming that the Rdi1–Cdc42 complex exists as a fraction of total cytosolic Cdc42, we find $R_c = \gamma v$, in which $0 < \gamma < 1$. Given conservation of total amount of Rdi1 (R) in the cell, we also have $R_f = R - R_c = R - \gamma v$. This means that both $R_c(x,t)$ and $R_f(x,t)$ are dependent on the Cdc42 dynamics.

Spatiotemporal dynamics of Cdc42 is described by the equations in the region $0 \le x \le L$:

$$\frac{\partial u}{\partial t} = \gamma A u^2 v - \beta u(R - \gamma v) + D_u \frac{\partial^2 u}{\partial x^2},$$

$$\frac{\partial v}{\partial t} = -\gamma A u^2 v + \beta u(R - \gamma v) + D_v \frac{\partial^2 v}{\partial x^2}, \quad (1)$$

in which the diffusion of the Cdc42 cytosolic form is much faster than the membrane one: $D_v >> D_u$. The cubic nonlinearity is shown to be critical for the Turing-type instability in polarization models (Goryachev and Pokhilko, 2008). The system of Eq. 1 is subject to no-flux boundary conditions. Summing up the equations and integrating over the spatial interval, we obtain the Cdc42 mass conservation condition

$$\int_0^L (u + v)\,dx = CL = \text{constant}, \quad (2)$$

in which the constant C is the model parameter representing the mean Cdc42 concentration. The reaction terms used in Eq. 1 lead to a basic uniform solution $u = 0$ corresponding to absence of Cdc42 on the membrane. To have some nonzero basal level u_b on the membrane, we modify the reaction term in Eq. 1 to arrive at

$$\frac{\partial u}{\partial t} = f(u,v) + D_u \frac{\partial^2 u}{\partial x^2},$$

$$\frac{\partial v}{\partial t} = -f(u,v) + D_v \frac{\partial^2 v}{\partial x^2},$$

$$f(u,v) = \gamma A(u - u_b)^2 v - \beta(u - u_b)(R - \gamma v). \quad (3)$$

Being stationary and spatially uniform, the solution $\{u_0, v_0\}$ is independent of time and spatial variables, so that all derivatives vanish, and this solution should satisfy the equation $f(u_0,v_0) = 0$. From Eq. 2, it follows that the basic solution satisfies the condition $u_0 + v_0 = C$, and we find from Eq. 3

$$u_0 = \frac{AC - \beta + Au_b - s}{2A},$$

$$v_0 = \frac{AC + \beta - Au_b + s}{2A},$$

$$s = \sqrt{(AC + \beta - Au_b)^2 - 4\beta AR/\gamma}. \quad (4)$$

As the uniform steady-state concentrations should be nonnegative, we find a necessary condition on the model parameters $R > \gamma C$, which was shown to be satisfied with experimental measurements and the estimated value of 0.4 for γ.

A previous study (Rubinstein et al., 2012) showed that the maximal linear growth rate σ_m of the perturbation can be approximated by the partial derivative of f with respect to the variable u: $\sigma_m \approx \partial f/\partial u = 2\gamma A(u_0 - u_b)v_0 - \beta(R - \gamma v_0)$, computed at the basic solution (Eq. 4). Meanwhile, the basic solution satisfies the relation $\gamma A(u_0 - u_b)v_0 = \beta(R - \gamma v_0)$, which produces an estimate for the growth rate for membrane Cdc42 in the form $\sigma_m \approx \beta(R - \gamma v_0) = \gamma A(u_0 - u_b)v_0$.

The last relation shows that the growth rate of membrane Cdc42, which determines the kinetics of polarization establishment, is proportional to the concentration of Rdi1 (R). It also depends on the activation level A, and more precisely, it is determined by the balance between the activation level A and the Rdi1 expression R.

For a fixed value of activation, with increase in R, the internalization term wins over the membrane-targeting term, eventually blocking polarization. On the other hand, for small $R < \gamma C$, polarization is also not possible. This means that there exists a range of the Rdi1 expression level R for which the polarization is possible, and the upper boundary of this range varies with A. This behavior is illustrated in Fig. 7 C in which the maximal value u_{max} of the membrane-bound Cdc42 concentration obtained by simulation of Eq. 3 is shown for a fixed value of A and increasing R. The nonpolarized state (with the ratio $u_{max}/u_{min} < 1.2$) is shown by the dashed curve. The parameter values used in this simulation are $C = 1$, $\gamma = 0.4$, $\beta = 0.2$, $D_v = 0.1$, $D_u = 0.01$, $u_b = 0.05$, and $L = 3$. The simulations for each set of the parameters were performed 25 times, and the mean values of u_{max} were computed.

Genetic manipulations

Site-directed mutagenesis was performed using the site-directed mutagenesis kit (QuikChange II XL; Agilent Technologies), and the final product was sequenced to ensure that there were no secondary mutations introduced. All yeast strains used in this study are described in Table S1. Techniques for yeast cell culture and genetics were essentially as previously described (Burke et al., 2000). Transformation of plasmid DNA into yeast was performed based on the lithium acetate method (Ito et al., 1983). Transformation of DNA fragments was performed by the same method, but after transformation, cells were recovered in nonselective media for at least two cell cycle times before plating on selective media, and genomic integration was confirmed by PCR. The plasmid DLB3170 was a gift from D. Lew (Duke University School of Medicine, Durham, NC).

α-Factor release assays

Cells were arrested at 23°C for 1.5 h using 20 µg/ml α-factor and released into the cell cycle by washing three times in sterile water before resuspending in fresh media with either 50 µM LatA or equivalent DMSO. LatA treatment was confirmed to result in actin polymerization within 15 min (Fig. S1 B). Samples containing Bem1-GFP or Cdc24-GFP were imaged as live cells 50 min after release. Samples were taken at 20, 50, and 80 min after release, fixed in 4% paraformaldehyde for 15 min before washing in PBS, and stored at 4°C for <48 h before imaging. For each time point, >80 cells were scored for polarity. The assay was repeated at least three times for each genotype. For release assays with Rdi1 expression induced under the Gal1 promoter, *pGAL1-RDI1* cells were grown overnight in 4% raffinose media, to which 4% galactose was added at the appropriate time point relative to the addition of α-factor such that addition of glucose 30 min before release from α-factor would end the induction.

Microscopy and live-cell imaging

Imaging was performed at 23°C on a spinning-disk confocal microscope (UltraVIEW; PerkinElmer), including an inverted microscope (Axiovert 200 M; Carl Zeiss), attached to a spinning-disk confocal system (CSU-X1; Yokogawa Corporation of America) and electron multiplying charge-coupled device (EM-CCD) camera (C9100; Hamamatsu Photonics) with Volocity acquisition software (PerkinElmer) or a similar system with MetaMorph acquisition software (Molecular Devices). Single time point images of live or fixed cells were collected as a series of optical sections, with a step size of 0.5 µm. ImageJ software (v. 1.37; National Institutes of Health) was used to process the images. Final images are maximum projections that have been background subtracted and contrast adjusted for clarity. Cdc24-GFP, Bem1-GFP, and mCherry-Cdc42 images were taken with a 100× αPlan Fluar, NA 1.46 objective lens, whereas GFP-Cdc42 and Cdc24-GFP-Cla4 images were taken with a 63× Plan Apochromat, NA 1.4 objective lens.

For live-cell videos of GFP-Cdc42, cells were arrested in G1 via pheromone for 1.5 h and released into LatA-containing synthetic complete (SC) media for 30 min before slide preparation on a 1% agarose and 100 µM LatA pad. Z-stack images were acquired at 30-s time intervals with 0.7 µm between slices. Maximum z projections of each time point were

generated, cells showing polar cap formation and disappearance within a single movie were identified, and the maximum intensity of the polar cap was measured and plotted over time. These were smoothed via a rolling mean of six time points and then fitted to Gaussian curves in OriginPro (OriginLab). The duration of the cap is reported as the full width half maximum of the Gaussian fit.

For live videos of Cdc24-GFP, cycling mid–log phase cells were immobilized on 1% agarose in SC media and imaged at 2-min time intervals as z-stack images with 0.7 µm between slices. Cells were aligned before kymograph generation by manually tracking either the polar cap or bud neck after bud emergence. Kymographs were then generated by averaging over a thickness of 3 pixels along the cortex using a custom plugin in ImageJ. This and other plugins can be found at the Stowers Institute ImageJ Plugins website and in a ZIP file provided online in Supplemental material.

Bem1 polarity analysis

Maximum projections of Bem1-GFP fluorescence images from the experiment in Fig. 2 I were background subtracted and processed using the ImageJ Smooth function to remove noise. Unbudded cells were circled, and the maximum and mean pixel intensities were calculated for a total of 520 cells per genotype. The Bem1 polarity was calculated as the maximum pixel intensity divided by the mean intensity per each cell.

Cdc24-GFP and mCherry-Cdc42 profile analysis

Two-channel z-stack images of cells expressing Cdc24-GFP and mCherry-Cdc42 were background subtracted, and maximum projections were generated. A cortex mask of the cell was then generated from the mCherry-Cdc42 channel using a custom macro based on the Li Dark thresholding algorithm in ImageJ (Li and Tam, 1998). The mask was applied to the Cdc24-GFP channel, and the mean intensity of the masked region in 10° increments around the cortex was calculated using a custom plug-in to generate a cortical intensity profile or Cdc24-GFP or similarly with the mCherry channel. This was completed for ≥15 cells, including all visibly polarized cells from each of several images. The profiles were aligned by maximum value, and each was normalized to the mean intensity of the cortex in the 180° region opposite the peak. The normalized curves were averaged. Statistical analysis was performed on peak (0°) values.

Cdc42 activation biosensor imaging and analysis

Cells were grown to mid–log phase before analysis. Polarized cells were imaged on a spinning-disk confocal microscope (UltraVIEW) including an inverted microscope (Axiovert 200 M), a spinning-disc confocal system (CSU-X1), a charge-coupled device (2 × 2 bin; ORCA-R2; Hamamatsu Photonics), and a PhotoKinesis accessory (PerkinElmer) using Volocity acquisition software with a 100× αPlan Fluar, NA 1.46 objective. Cells were imaged at maximum speed for a total of 42 frames, with 488-nm laser power at 7% and exposure at 100–300 ms depending on biosensor expression level per cell. mCherry throughout the cell was bleached after frame 20, using one iteration of 568-nm laser at 100%. mCherry fluorescence was checked after acquisition to ensure complete bleaching. Controls indicated no significant bleaching of GFP by 568-nm excitation nor cross talk of mCherry fluorescence into the GFP channel. The sensor was expressed within a similar range (measured by fluorescence) in all strains, and cortical fluorescence intensity did not correlate with FRET (Fig. S2). Analysis was performed using ImageJ software. The first two frames after bleaching (frames 21–22) were discarded because of a potential delay of 568-nm laser shut off. The sum of the full time series was then used to create a cortex mask of the cell, using a custom macro based on the Li Dark thresholding algorithm in ImageJ (see Supplemental material; Li and Tam, 1998). The mask was applied to the series, and the mean intensity of the masked region in 10° increments around the cortex was calculated at each time point using a custom plug-in. The mean intensity and the SD intensity of each 10° increment before and after bleach were calculated in RStudio (RStudio, Inc.). The SDs of all 10° increments before and after bleach were averaged, and cells whose mean SD was >10% of its mean cortical fluorescence were discarded. Intensity profiles of remaining cells were then aligned such that polar cap center was located at 0°. FRET efficiency was calculated for each 10° segment in remaining cells as 100 × (postbleach − prebleach)/prebleach. FRET efficiencies for each 10° increment were then averaged over ≥25 cells, as in the plot in Fig. 4 C. The peak FRET efficiency (Fig. 4 D) was determined as the mean of the 30° region containing the 10° increment of highest mean FRET efficiency among aligned profiles, as illustrated by the yellow box in Fig. 4 C.

Statistical analysis

Statistical differences between two sets of data were analyzed with a two-tailed unpaired Student's *t* test.

Online supplemental material

Fig. S1 shows additional data for characterization of spatial cue independent polarization backgrounds, *rsr1Δ* and *axl2Δ rax1Δ*. Fig. S2 shows mean cortical intensity of the Cdc42 biosensor plotted against FRET efficiency for each cell in the analysis. Fig. S3 shows a schematic of the experimental procedure used to generate Fig. 7 D and the relative levels of Rdi1 and Cdc42. Videos 1 and 2 show polar cap dynamics of GFP-Cdc42 in LatA in an *rsr1Δ* cell and an *axl2Δ rax1Δ* cell, respectively. Videos 3 and 4 show localization of Cdc24-GFP during budding in *rsr1Δ bem1Δ* cells and *axl2Δ rax1Δ bem1Δ* cells, respectively. Table S1 shows yeast strains used in this study. A ZIP file is also provided that contains custom plug-ins and macros written for ImageJ, used to calculate cortical intensity profiles and kymographs. Online supplemental material is available at http://www.jcb.org/cgi/content/full/jcb.201304180/DC1.

The authors thank J. Zhu, W. Mulla, V. Ramalingam, J. Lange, W. Bradford, S. Ramachandran, G. Rancati, S. Wai, and X. Fan (all current or former Stowers Institute members) for experimental assistance and valuable discussion and D. Lew for the plasmid DLB3170.

This work was supported by a National Institutes of Health grant GM-RO1-057063 awarded to R. Li.

Submitted: 26 April 2013
Accepted: 22 August 2013

References

Altschuler, S.J., S.B. Angenent, Y. Wang, and L.F. Wu. 2008. On the spontaneous emergence of cell polarity. *Nature*. 454:886–889. http://dx.doi.org/10.1038/nature07119

Ayscough, K.R., J. Stryker, N. Pokala, M. Sanders, P. Crews, and D.G. Drubin. 1997. High rates of actin filament turnover in budding yeast and roles for actin in establishment and maintenance of cell polarity revealed using the actin inhibitor latrunculin-A. *J. Cell Biol.* 137:399–416. http://dx.doi.org/10.1083/jcb.137.2.399

Bender, L., H.S. Lo, H. Lee, V. Kokojan, V. Peterson, and A. Bender. 1996. Associations among PH and SH3 domain-containing proteins and Rho-type GTPases in Yeast. *J. Cell Biol.* 133:879–894. http://dx.doi.org/10.1083/jcb.133.4.879

Bose, I., J.E. Irazoqui, J.J. Moskow, E.S.G. Bardes, T.R. Zyla, and D.J. Lew. 2001. Assembly of scaffold-mediated complexes containing Cdc42p, the exchange factor Cdc24p, and the effector Cla4p required for cell cycle-regulated phosphorylation of Cdc24p. *J. Biol. Chem.* 276:7176–7186. http://dx.doi.org/10.1074/jbc.M010546200

Burke, D., D. Dawson, and T. Stearns. 2000. Methods in Yeast Genetics: a Cold Spring Harbor Laboratory Course Manual. Cold Spring Harbor Laboratory Press, Plainview, NY. 205 pp.

Butty, A.-C., N. Perrinjaquet, A. Petit, M. Jaquenoud, J.E. Segall, K. Hofmann, C. Zwahlen, and M. Peter. 2002. A positive feedback loop stabilizes the guanine-nucleotide exchange factor Cdc24 at sites of polarization. *EMBO J.* 21:1565–1576. http://dx.doi.org/10.1093/emboj/21.7.1565

Casamayor, A., and M. Snyder. 2002. Bud-site selection and cell polarity in budding yeast. *Curr. Opin. Microbiol.* 5:179–186. http://dx.doi.org/10.1016/S1369-5274(02)00300-4

Das, A., B.D. Slaughter, J.R. Unruh, W.D. Bradford, R. Alexander, B. Rubinstein, and R. Li. 2012. Flippase-mediated phospholipid asymmetry promotes fast Cdc42 recycling in dynamic maintenance of cell polarity. *Nat. Cell Biol.* 14:304–310. http://dx.doi.org/10.1038/ncb2444

DerMardirossian, C., and G.M. Bokoch. 2005. GDIs: central regulatory molecules in Rho GTPase activation. *Trends Cell Biol.* 15:356–363. http://dx.doi.org/10.1016/j.tcb.2005.05.001

Etienne-Manneville, S. 2004. Cdc42—the centre of polarity. *J. Cell Sci.* 117:1291–1300. http://dx.doi.org/10.1242/jcs.01115

Freisinger, T., B. Klünder, J. Johnson, N. Müller, G. Pichler, G. Beck, M. Costanzo, C. Boone, R.A. Cerione, E. Frey, and R. Wedlich-Söldner. 2013. Establishment of a robust single axis of cell polarity by coupling multiple positive feedback loops. *Nat. Commun.* 4:1807. http://dx.doi.org/10.1038/ncomms2795

Fujita, A., M. Lord, T. Hiroko, F. Hiroko, T. Chen, C. Oka, Y. Misumi, and J. Chant. 2004. Rax1, a protein required for the establishment of the bipolar budding pattern in yeast. *Gene*. 327:161–169. http://dx.doi.org/10.1016/j.gene.2003.11.021

Gao, X.-D., L.M. Sperber, S.A. Kane, Z. Tong, A.H.Y. Tong, C. Boone, and E. Bi. 2007. Sequential and distinct roles of the cadherin domain-containing protein Axl2p in cell polarization in yeast cell cycle. *Mol. Biol. Cell*. 18:2542–2560. http://dx.doi.org/10.1091/mbc.E06-09-0822

Goehring, N.W., P.K. Trong, J.S. Bois, D. Chowdhury, E.M. Nicola, A.A. Hyman, and S.W. Grill. 2011. Polarization of PAR proteins by advective triggering of a pattern-forming system. *Science*. 334:1137–1141. http://dx.doi.org/10.1126/science.1208619

Goryachev, A.B., and A.V. Pokhilko. 2006. Computational model explains high activity and rapid cycling of Rho GTPases within protein complexes. *PLOS Comput. Biol.* 2:e172. http://dx.doi.org/10.1371/journal.pcbi.0020172

Goryachev, A.B., and A.V. Pokhilko. 2008. Dynamics of Cdc42 network embodies a Turing-type mechanism of yeast cell polarity. *FEBS Lett.* 582:1437–1443. http://dx.doi.org/10.1016/j.febslet.2008.03.029

Gulli, M.-P., M. Jaquenoud, Y. Shimada, G. Niederhäuser, P. Wiget, and M. Peter. 2000. Phosphorylation of the Cdc42 exchange factor Cdc24 by the PAK-like kinase Cla4 may regulate polarized growth in yeast. *Mol. Cell*. 6:1155–1167. http://dx.doi.org/10.1016/S1097-2765(00)00113-1

Hodgson, L., O. Pertz, and K.M. Hahn. 2008. Design and optimization of genetically encoded fluorescent biosensors: GTPase biosensors. *Methods Cell Biol.* 85:63–81. http://dx.doi.org/10.1016/S0091-679X(08)85004-2

Howell, A.S., N.S. Savage, S.A. Johnson, I. Bose, A.W. Wagner, T.R. Zyla, H.F. Nijhout, M.C. Reed, A.B. Goryachev, and D.J. Lew. 2009. Singularity in polarization: rewiring yeast cells to make two buds. *Cell*. 139:731–743. http://dx.doi.org/10.1016/j.cell.2009.10.024

Howell, A.S., M. Jin, C.F. Wu, T.R. Zyla, T.C. Elston, and D.J. Lew. 2012. Negative feedback enhances robustness in the yeast polarity establishment circuit. *Cell*. 149:322–333. http://dx.doi.org/10.1016/j.cell.2012.03.012

Irazoqui, J.E., A.S. Gladfelter, and D.J. Lew. 2003. Scaffold-mediated symmetry breaking by Cdc42p. *Nat. Cell Biol.* 5:1062–1070. http://dx.doi.org/10.1038/ncb1068

Ito, H., Y. Fukuda, K. Murata, and A. Kimura. 1983. Transformation of intact yeast cells treated with alkali cations. *J. Bacteriol.* 153:163–168.

Ito, T., Y. Matsui, T. Ago, K. Ota, and H. Sumimoto. 2001. Novel modular domain PB1 recognizes PC motif to mediate functional protein-protein interactions. *EMBO J.* 20:3938–3946. http://dx.doi.org/10.1093/emboj/20.15.3938

Itoh, R.E., K. Kurokawa, Y. Ohba, H. Yoshizaki, N. Mochizuki, and M. Matsuda. 2002. Activation of rac and cdc42 video imaged by fluorescent resonance energy transfer-based single-molecule probes in the membrane of living cells. *Mol. Cell. Biol.* 22:6582–6591. http://dx.doi.org/10.1128/MCB.22.18.6582-6591.2002

Jose, M., S. Tollis, D. Nair, J.-B. Sibarita, and D. McCusker. 2013. Robust polarity establishment occurs via an endocytosis-based cortical corralling mechanism. *J. Cell Biol.* 200:407–418. http://dx.doi.org/10.1083/jcb.201206081

Kang, P.J., L. Béven, S. Hariharan, and H.-O. Park. 2010. The Rsr1/Bud1 GTPase interacts with itself and the Cdc42 GTPase during bud-site selection and polarity establishment in budding yeast. *Mol. Biol. Cell*. 21:3007–3016. http://dx.doi.org/10.1091/mbc.E10-03-0232

Koch, G., K. Tanaka, T. Masuda, W. Yamochi, H. Nonaka, and Y. Takai. 1997. Association of the Rho family small GTP-binding proteins with Rho GDP dissociation inhibitor (Rho GDI) in *Saccharomyces cerevisiae*. *Oncogene*. 15:417–422. http://dx.doi.org/10.1038/sj.onc.1201194

Kozminski, K.G., L. Beven, E. Angerman, A.H.Y. Tong, C. Boone, and H.-O. Park. 2003. Interaction between a Ras and a Rho GTPase couples selection of a growth site to the development of cell polarity in yeast. *Mol. Biol. Cell*. 14:4958–4970. http://dx.doi.org/10.1091/mbc.E03-06-0426

Kozubowski, L., K. Saito, J.M. Johnson, A.S. Howell, T.R. Zyla, and D.J. Lew. 2008. Symmetry-breaking polarization driven by a Cdc42p GEF-PAK complex. *Curr. Biol.* 18:1719–1726. http://dx.doi.org/10.1016/j.cub.2008.09.060

Ku, C.-J., Y. Wang, O.D. Weiner, S.J. Altschuler, and L.F. Wu. 2012. Network crosstalk dynamically changes during neutrophil polarization. *Cell*. 149:1073–1083. http://dx.doi.org/10.1016/j.cell.2012.03.044

Larson, S.M., and A.R. Davidson. 2000. The identification of conserved interactions within the SH3 domain by alignment of sequences and structures. *Protein Sci.* 9:2170–2180. http://dx.doi.org/10.1110/ps.9.11.2170

Li, C.H., and P.K.S. Tam. 1998. An iterative algorithm for minimum cross entropy thresholding. *Pattern Recognit. Lett.* 18:771–776. http://dx.doi.org/10.1016/S0167-8655(98)00057-9

Li, R., and G.G. Gundersen. 2008. Beyond polymer polarity: how the cytoskeleton builds a polarized cell. *Nat. Rev. Mol. Cell Biol.* 9:860–873. http://dx.doi.org/10.1038/nrm2522

Marco, E., R. Wedlich-Soldner, R. Li, S.J. Altschuler, and L.F. Wu. 2007. Endocytosis optimizes the dynamic localization of membrane proteins that regulate cortical polarity. *Cell*. 129:411–422. http://dx.doi.org/10.1016/j.cell.2007.02.043

McCaffrey, L.M., and I.G. Macara. 2009. Widely conserved signaling pathways in the establishment of cell polarity. *Cold Spring Harb. Perspect. Biol.* 1:a001370. http://dx.doi.org/10.1101/cshperspect.a001370

Mori, Y., A. Jilkine, and L. Edelstein-Keshet. 2011. Asymptotic and bifurcation analysis of wave-pinning in a reaction-diffusion model for cell plarization. *SIAM J. Appl. Math.* 71:1401–1427. http://dx.doi.org/10.1137/10079118X

Onsum, M.D., and C.V. Rao. 2009. Calling heads from tails: the role of mathematical modeling in understanding cell polarization. *Curr. Opin. Cell Biol.* 21:74–81. http://dx.doi.org/10.1016/j.ceb.2009.01.001

Otsuji, M., S. Ishihara, C. Co, K. Kaibuchi, A. Mochizuki, and S. Kuroda. 2007. A mass conserved reaction-diffusion system captures properties of cell polarity. *PLOS Comput. Biol.* 3:e108. http://dx.doi.org/10.1371/journal.pcbi.0030108

Ozbudak, E.M., A. Becskei, and A. van Oudenaarden. 2005. A system of counteracting feedback loops regulates Cdc42p activity during spontaneous cell polarization. *Dev. Cell*. 9:565–571. http://dx.doi.org/10.1016/j.devcel.2005.08.014

Park, H.-O., and E. Bi. 2007. Central roles of small GTPases in the development of cell polarity in yeast and beyond. *Microbiol. Mol. Biol. Rev.* 71:48–96. http://dx.doi.org/10.1128/MMBR.00028-06

Park, H.-O., E. Bi, J.R. Pringle, and I. Herskowitz. 1997. Two active states of the Ras-related Bud1/Rsr1 protein bind to different effectors to determine yeast cell polarity. *Proc. Natl. Acad. Sci. USA*. 94:4463–4468. http://dx.doi.org/10.1073/pnas.94.9.4463

Park, H.-O., P.J. Kang, and A.W. Rachfal. 2002. Localization of the Rsr1/Bud1 GTPase involved in selection of a proper growth site in yeast. *J. Biol. Chem.* 277:26721–26724. http://dx.doi.org/10.1074/jbc.C200245200

Peterson, J., Y. Zheng, L. Bender, A. Myers, R. Cerione, and A. Bender. 1994. Interactions between the bud emergence proteins Bem1p and Bem2p and Rho-type GTPases in yeast. *J. Cell Biol.* 127:1395–1406. http://dx.doi.org/10.1083/jcb.127.5.1395

Roemer, T., K. Madden, J. Chang, and M. Snyder. 1996. Selection of axial growth sites in yeast requires Axl2p, a novel plasma membrane glycoprotein. *Genes Dev.* 10:777–793. http://dx.doi.org/10.1101/gad.10.7.777

Rubinstein, B., B.D. Slaughter, and R. Li. 2012. Weakly nonlinear analysis of symmetry breaking in cell polarity models. *Phys. Biol.* 9:045006. http://dx.doi.org/10.1088/1478-3975/9/4/045006

Sanders, S.L., M. Gentzsch, W. Tanner, and I. Herskowitz. 1999. O-Glycosylation of Axl2/Bud10p by Pmt4p is required for its stability, localization, and function in daughter cells. *J. Cell Biol.* 145:1177–1188. http://dx.doi.org/10.1083/jcb.145.6.1177

Savage, N.S., A.T. Layton, and D.J. Lew. 2012. Mechanistic mathematical model of polarity in yeast. *Mol. Biol. Cell*. 23:1998–2013. http://dx.doi.org/10.1091/mbc.E11-10-0837

Seetapun, D., and D.J. Odde. 2010. Cell-length-dependent microtubule accumulation during polarization. *Curr. Biol.* 20:979–988. http://dx.doi.org/10.1016/j.cub.2010.04.040

Shimada, Y., P. Wiget, M.-P. Gulli, E. Bi, and M. Peter. 2004. The nucleotide exchange factor Cdc24p may be regulated by auto-inhibition. *EMBO J.* 23:1051–1062. http://dx.doi.org/10.1038/sj.emboj.7600124

Slaughter, B.D., A. Das, J.W. Schwartz, B. Rubinstein, and R. Li. 2009. Dual modes of cdc42 recycling fine-tune polarized morphogenesis. *Dev. Cell*. 17:823–835. http://dx.doi.org/10.1016/j.devcel.2009.10.022

Slaughter, B.D., J.R. Unruh, A. Das, S.E. Smith, B. Rubinstein, and R. Li. 2013. Non-uniform membrane diffusion enables steady-state cell polarization via vesicular trafficking. *Nat Commun*. 4:1380. http://dx.doi.org/10.1038/ncomms2370

Tiedje, C., I. Sakwa, U. Just, and T. Höfken. 2008. The Rho GDI Rdi1 regulates Rho GTPases by distinct mechanisms. *Mol. Biol. Cell*. 19:2885–2896. http://dx.doi.org/10.1091/mbc.E07-11-1152

van Drogen-Petit, A., C. Zwahlen, M. Peter, and A.M.J.J. Bonvin. 2004. Insight into molecular interactions between two PB1 domains. *J. Mol. Biol.* 336:1195–1210. http://dx.doi.org/10.1016/j.jmb.2003.12.062

Wai, S.C., S.A. Gerber, and R. Li. 2009. Multisite phosphorylation of the guanine nucleotide exchange factor Cdc24 during yeast cell polarization. *PLoS ONE*. 4:e6563. http://dx.doi.org/10.1371/journal.pone.0006563

Wedlich-Soldner, R., S. Altschuler, L. Wu, and R. Li. 2003. Spontaneous cell polarization through actomyosin-based delivery of the Cdc42 GTPase. *Science*. 299:1231–1235. http://dx.doi.org/10.1126/science.1080944

Wedlich-Soldner, R., S.C. Wai, T. Schmidt, and R. Li. 2004. Robust cell polarity is a dynamic state established by coupling transport and GTPase signaling. *J. Cell Biol.* 166:889–900. http://dx.doi.org/10.1083/jcb.200405061

Yamaguchi, Y., K. Ota, and T. Ito. 2007. A novel Cdc42-interacting domain of the yeast polarity establishment protein Bem1. Implications for modulation of mating pheromone signaling. *J. Biol. Chem.* 282:29–38. http://dx.doi.org/10.1074/jbc.M609308200

Zheng, Y., A. Bender, and R.A. Cerione. 1995. Interactions among proteins involved in bud-site selection and bud-site assembly in *Saccharomyces cerevisiae*. *J. Biol. Chem.* 270:626–630. http://dx.doi.org/10.1074/jbc.270.2.626